Strength Design Analysis of Corrugated Board

Nyman, Ulf

2000

Document Version:
Publisher's PDF, also known as Version of record

LUND UNIVERSITY

STRENGTH DESIGN ANALYSIS OF CORRUGATED BOARD

ULF NYMAN

Department of Mechanics and Materials

Structural Mechanics

Licentiate Dissertation

Department of Mechanics and Materials
Structural Mechanics

ISRN LUTVDG/TVSM--00/3048--SE (1-68)
ISSN 0281-6679

STRENGTH DESIGN ANALYSIS OF CORRUGATED BOARD

ULF NYMAN

Printed by KFS i Lund AB, Lund, Sweden. June 2000.

For information, address:
Division of Structural Mechanics, LTH, Lund University, Box 118, SE-221 00 Lund, Sweden.
Homepage: http://www.byggmek.lth.se

Preface

The work presented in this licentiate thesis was carried out at the Division of Structural Mechanics, Department of Mechanics and Materials, Lund University.

The outcome of the research is a portion of a participating program with FPIRC, Forest Products Industry Research College. The economic support from the Foundation for Strategic Research (SSF), Forest Products Industry Research College program and from Bo Rydins stiftelse för vetenskaplig forskning is gratefully acknowledged.

I would like to express my gratitude to my supervisor, Doc. Per Johan Gustafsson, for his support and for the moments of dedicated discussions. He made a large contribution to this work by sharing his thoughts and giving valuable comments. I also would like to thank Prof. Göran Sandberg for his encouragement for the continuation of the work. Mr. Bo Zadig, thank you for help with completion of the figures.

There is of course a multitude of people and collegues at Structural Mechanics, who contributed in some way to the work. For example M. Sc. Peter Davidsson, who I shared room with, shared a lot of tips about the computer system use. Thank you other, all of whom contributed with valuable tips and comments.

Finally, I am grateful for the advantage of the computational resources, furnished by Lunarc, Center for Scientific and Technical Computing.

Lund, June 2000

Ulf Nyman

Contents

Summary of papers 1-4

Introduction

Paper 1 U. Nyman, P. J. Gustafsson, *Buckling of Long Orthotropic Plates Including Higher-Order Transverse Shear*, Submitted to J. of Engineering Mechanics

Paper 2 U. Nyman and P. J. Gustafsson, *Local Buckling of Corrugated Board Facings*, Proceedings of the European Conference on Computational Mechanics, Munchen, Germany, (1999)

Paper 3 U. Nyman, P. J. Gustafsson, *Material and Structural Failure Criterion of Corrugated Board Facings*, Composite Structures, Accepted for publication

Paper 4 U. Nyman, *Multilayer Reliability Analysis of Corrugated Board*, Report, TVSM-3049, Strctural Mechanics, Lund University (2000)

Summary of paper 1-4

Paper 1 The problem of buckling of long orthotropic plates under combined in-plane loading is considered. An approximate analytical solution is presented. The concept of a mixed Rayleigh-Ritz method is used considering higher-order shear deformations. The achieved load function of the half buckling wavelength and the inclination of the nodal lines is minimized via a simplex search method. For low transverse shear stiffnesses the model predicts buckling coefficients under in-plane shear load that are of the same order of magnitude as those resulting from a uniaxial compressive load. For a thin plate the critical shear load is larger by 42% compared to the uniaxial case. The model also suggests that for highly anisotropic materials, such as paper, the critical load solution is still influenced by the shear deformation effect at width-to-thickness ratios above 100.

Paper 2 Local buckling of corrugated board facings is studied numerically through finite element calculations. In addition, an analytical model is developed by the use of the Rayleigh-Ritz method. The facings are modeled as infinite orthotropic plates, resting on parallel free supports and subjected to an arbitrary in-plane stress state. The deflection shape is defined by wave length and displacement of the periodic deflection pattern. Transverse shear strain is considered by first (FEM) and higher order (analytical) shape functions. The results suggest that the low out-of-plane shear stiffness of paper significantly affect the critical load.

Paper 3 A failure stress criterion for corrugated board facings is presented. The failure criterion is based on material failure and structural local buckling failure, which are evaluated in a combined analysis procedure. The failure stress is compared with collapse experiments on corrugated board cylinders and the failure stress presented herein is seen to be in much better agreement with the measured stresses than the Tsai-Wu failure criterion alone. The fluting wavelength of the corrugated board is also varied for the purpose of strength sensitivity analysis of corrugated board.

Paper 4 The reliability of corrugated board is studied by finite element Monte Carlo simulations and by a first order reliability method, with the use of a failure criterion that includes both material failure and structural failure. The stiffness and strength parameters of the board are given as scalar multipliers of a geometrically distributed stochastic field. For the case of pure bending stresses, it is concluded that the failure is almost completely governed by structural failure. It is also seen that the board is very sensitive to compressive stresses in the machine direction (MD).

Introduction

Background

Corrugated board is a light-weight structural sandwich material. Typically, it is found in applications as corrugated containers for the storage and distribution of larger consumer products or provisions, see Figure 1. In some cases, the board is found in applications where its function is purely to act as a load bearing structure, for example as pallets, see Figure 2. Hence, it is important that the board mechanical properties meet the desired properties of the user.

Figure 1: Stack of corrugated containers.

Figure 2: Corrugated board pallets.

The design of corrugated board, in terms of material strength and overall load resistance, has formerly been devoted to empirical research and relatively simple models. One example of an empirical result is the formula for box compression strength proposed by Maltenfort [1], which is derived from statistical data from tests of box compression strength. At present, there are numerous general purpose finite element codes for the

evaluation of stress distributions, facilitating work on more theoretical and rational methods for strength analysis. Studies of the strength of corrugated board based on structural analysis has been performed by Patel [4], who both numerically and experimentally examined the biaxial strength, and by Nordstrand et. al. [5, 6], who derived expressions for the shear stiffness of the board and studied the postbuckling strength of the board. It was found that the failure of the board is largely influenced by local instability of the facing and a strength analysis based solely on material failure therefore is an insufficent representation of the ultimate strength.

The strength of corrugated board due to localized buckling was previously studied by Johnson and Urbanik [7]. In the work, a non-linear finite element method was used to examine the instability. Furthermore, Johnson and Urbanik [8] developed a non-linear elastic plate theory with the application to paper bending properties.

Corrugated board is largely affected by environmental conditions, such as moisture exposure. For example, a paper sheet holding 15% moisture content, which corresponds to 70-80% relative humidity (RH), will only preserve one half of its dry stiffness [3]. The mechanical characteristics of corrugated board is to a large extent retaining uncertainties. These uncertainties relate to

- Material properties; e.g. elastic stiffness and material strength
- Geometric properties; such as geometrical imperfections of the panels
- Loads; stack height, duration of load, mishandling of packages etc.
- Environmental conditions; magnitude and variation of RH, risk of wet material etc.

Therefore, for a reliable design analysis, it appears natural to incorporate uncertainties in a strength analysis. In such an analysis, the physical variation in material properties with varying climate conditions can be modelled.

Many different techniques for the study of structural reliability are availible. The techniques can be categorized as exact, e.g. Monte Carlo methods, multifold integral evaluation, and approximate, e.g. series expansion methods, response surface fitting and FORM/SORM (First/Second Order Reliability Methods.

In using the Monte Carlo method, a suitable number of samples are created as input variables to the structural model. The computation effort with this method is obvious and will, of course, increase with the effort needed for the basic deterministic model. In contrary, it is the most versatile method in terms of problem definition and the solution is always convergent. In order to reduce the computational effort, different methods to reduce the number of samples in structural analysis has been proposed, e.g. Olsson [2]. In using FORM or SORM, limit state functions are formulated which contain both the structural permissible response and the response as a function of load. The next step is to determine the probability content in terms of a minimization procedure. The attractivness of FORM/SORM lies in the comparably speed by which an engineering solution is attained. However, the method has mostly found its application on simple structures and the application to finite element methods is currently an intensive research field. Examples of work within reliability finite element analysis are Frangopol et. al. [9], Liu and Liu [10], Guan and Melchers [12], and Viadero et. al. [13].

Scope and observations of the present work

The three or more layers of paper that build up corrugated board are characterized by orthotropic material properties, similar to those which can be found in fiber reinforced polymer composites. The detailed geometry of the board is complex and the number of corrugations in the panels that forms a package is large. This makes detailed three-dimensional modelling of the corrugations unsuitable in strength analysis. In this work, it is the aim to use a simplified model, such as a laminated composite plate or shell finite element, for the analysis.

The failure of corrugated board is devoted to material failure and structural failure of the facing. Material failure occurs when either the fiber strength threshold is exceeded, or the bonds between the fibers no longer are able to carry load. Structural failure occurs when either of the facing becomes unstable, local buckling, see Figure 3.

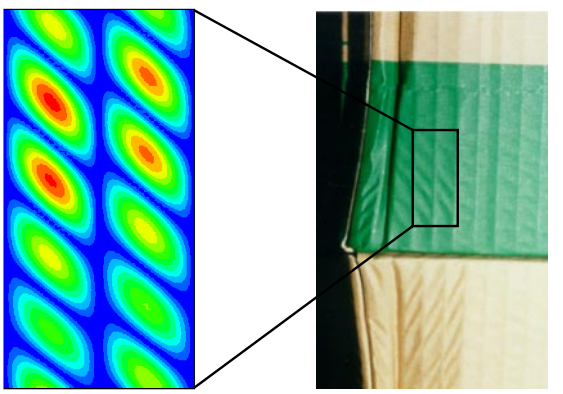

Figure 3: Shear buckling of facing.

The work presented herein comprises two parts. The initial part of the work studies the local instability of the board in an analytical manner (paper 1). In this first part, also finite element calculations are performed for evaluation (paper 2) and a combined failure criterion, involving both structural and material failure, is formulated (paper 3).

It is observed through the work that even though the paper sheets of the board are very thin, the high degree of orthotropy emphasizes the use of plate theories that enable out-of-plane shear deformation, in the analysis.

The second part of the present work is devoted to an examination of the applicability of FORM to the finite element analysis of plate structures (paper 4). The methodology mainly described in [14] is used and implemented together with the finite element method. As a comparison, Monte Carlo sampling is used. As a continuation of the third paper, the likeliness of either material or structural failure is examined. The stress failure criterion from paper 3, for determination of the ultimate strength of the board, is used in a limit state function including both the allowable local stress and the calculated local stress. The evaluation of the limit state function is performed by finite element calculations on a homogenisized laminated plate.

It is also the purpose of the paper to discern which method is most appropriate in a

continued work, in terms of accuracy, complexity and numerical efficiency. The uncertainties modelled in the last paper involve variations in the components of the stiffness matrix as well as the orthotropic material strength parameters.

It is the aim that the continued work will lead to a method applicable to reliability design of corrugated board packages. As the most common loading condition is shell like, it is crucial that the model incorporates geometrical non-linearities. It is of course also crucial to incorporate uncertainties in the loading conditions. Uncertainties in humidity conditions, geometrical imperfections and material non-linearities may also be of importance.

Introduction to the first order reliability method

Traditionally, strength analysis of structural systems has been devoted to a deterministic analysis, finding appropriate response measures and relating them to given strength conditions. However, in all practical structures, there are certain degree of variabilities in the variables affecting the strength and response. This can be accounted for by adding a factor of safety to the system and, prospectively, the strength will not be exceeded. A more detailed modelling is to use a mathematical description of the variable fluctuations and determine the probability that the strength will be exceeded. The probability of failure P_f, can in terms of the stochastic basic variables $\boldsymbol{\alpha}$, be written

$$P_f = P[g_\alpha(\boldsymbol{\alpha}) \leq 0] = \int_{g_\alpha(\boldsymbol{\alpha})\leq 0} f(\boldsymbol{\alpha}) d\alpha \tag{1}$$

where $g(\boldsymbol{\alpha})$ is the limit state function, which is positive when the structure is in a safe state, and $f(\boldsymbol{\alpha})$ is the joint probability density function of $\boldsymbol{\alpha}$. The general solution of the multifold integral in (1) provides a prohibitive task, which has led to the development of approximate techniques. One of the approximate techniques is FORM, in which the limit state function can be mapped to the standard uncorrelated normal space of the basic variables

$$T: \quad g_{\hat{\alpha}} \leq 0 \quad \rightarrow \quad g_z \leq 0 \tag{2}$$

where $\mathbf{z}$ are the standard normal variables and $\hat{\boldsymbol{\alpha}}$ is the set of uncorrelated basic variables. According to the mapping given by Hasofer and Lind, [15], the relation between $\mathbf{z}$ and $\hat{\boldsymbol{\alpha}}$ reads

$$\mathbf{z} = \hat{\mathbf{C}}_\alpha^{-1/2} \left(\hat{\boldsymbol{\alpha}} - \mathrm{E}[\hat{\boldsymbol{\alpha}}]\right) \tag{3}$$

The uncorrelated basic variables are related to $\boldsymbol{\alpha}$ by the orthogonal transformation matrix $\mathbf{A}$

$$\hat{\boldsymbol{\alpha}} = \mathbf{A}^T \boldsymbol{\alpha} \tag{4}$$

so that the covariance matrix $\hat{\mathbf{C}}_\alpha$ is diagonal

$$\hat{\mathbf{C}}_\alpha = \mathbf{A}^T \mathbf{C}_\alpha \mathbf{A} \tag{5}$$

In using FORM, the reliability index, β, is found as the minimum distance from the origin to the failure surface $g_z(\mathbf{z}) = 0$. This is expressed as

$$\beta = \min \|\mathbf{z}\| \quad \mathbf{z} \in L_z \tag{6}$$

where L_z defines the failure surface. The point in the z-coordinate system where the minimum distance is found is referred to as the design point. This point is found by the use of an iterative search algorithm.

For a generic failure surface, an approximation to the probability of failure is given by

$$P_f = \Phi(-\beta) \tag{7}$$

where Φ is the standard normal distribution function.

Implemented iterative search algorithm

There are many availible iterative algorithms for constrained minimization problems. A search algorithm which is found to be practical in structural minimization problems and used for the calculations presented in paper 4, is described in [14]. This algorithm uses the projection of the current point $\mathbf{z}^{(k)}$ on the failure surface gradient in a sequence of values of $\mathbf{z}$. The gradient pointing towards the failure region can be expressed as

$$\tilde{\mathbf{z}}^{(k)} = -\frac{\partial g(z^{(k)})/\partial z_i}{\left[\sum_{i=1}^{n} \left(\partial g(z^{(k)})/\partial z_i\right)^2\right]^{1/2}} \tag{8}$$

where n is the number of stochastic variables. The projection of $\mathbf{z}^{(k)}$ on $\tilde{\mathbf{z}}^{(k)}$ is given by

$$\mathbf{v}_a^{(k)} = (\mathbf{z}^{(k)} \cdot \tilde{\mathbf{z}}^{(k)})\tilde{\mathbf{z}}^{(k)} \tag{9}$$

The point at the end of this vector is put closer to the actual failure surface $g_z(\mathbf{z}) = 0$ by

$$\mathbf{v}_b^{(k)} = \frac{g(\mathbf{z}^{(k)})}{\left[\sum_{i=1}^{n} \left(\partial g(z^k)/\partial z_i\right)^2\right]^{1/2}} \tilde{\mathbf{z}}^{(k)} \tag{10}$$

The next iteration point is then given by

$$\mathbf{z}^{(k+1)} = \mathbf{v}_a^{(k)} + \mathbf{v}_b^{(k)} \tag{11}$$

and the iterations are continued until the convergence criterion

$$\begin{aligned} \|\mathbf{z}^{(k+1)} - \mathbf{z}^{(k)}\| &\leq \epsilon_1 \\ |g(\mathbf{z}^{(k+1)})| &\leq \epsilon_2 \end{aligned} \tag{12}$$

is fulfilled.

At the point of convergence, z^*, the limit surface can be given as a linearized surface, which has the equation

$$\sum_{i=1}^{n} \frac{\partial g(z^*)}{\partial z_i}(z_i - z_i^*) - g^* = 0 \tag{13}$$

or on normal form

$$\frac{1}{\left[\sum_{i=1}^{n} \left(\partial g(z^*)/\partial z_i\right)^2\right]^{1/2}} \sum_{i=1}^{n} \frac{\partial g(z^*)}{\partial z_i} z_i + \beta - g^* = 0 \tag{14}$$

It should be pointed out that if the limit state function is a convex function with very large curvature, the projection given by (9) will be directed to a point far apart from the limit state surface, and the solution is not convergent. If the failure criterion is a concave and closed function, the algorithm can be expected to converge to the design point.

References

[1] Maltenfort, G. G., (1956) *Compression Strength of Corrugated Containers*, Fibre Containers, Vol. 41, No. 7.

[2] Olsson, A., (1999) *Modelling Damage and Stochastic Properties in Engineering Structures*, Licentiate thesis, Dept. of Struc. Mech., Lund University.

[3] Salmen, L., (1982) *Temperature and Water Induced Softening Behaviour of Wood Fiber Based Materials*, Ph. D. thesis, Dept. of Paper Technology, KTH, Stockholm.

[4] Patel, P., (1996) *Biaxial Failure of Corrugated Board*, Licentiate thesis, Dept. of Eng. Logistics, Lund University.

[5] Nordstrand, T., Carlsson, L. A., and Allen, H. G., (1994) *Transverse Shear Stiffness of Structural Core Sandwich*, Composite Structures, **27**, pp 317-329.

[6] Nordstrand, T. M., (1995) *Parametric Study of the Post-Buckling Strength of Structural Core Sandwich Panels*, Composite Structures, **30**, pp 441-451.

[7] Johnson, M. W., and Urbanik, T. J., (1989) *Analysis of the Localized Buckling in Composite Plate Structures with application to Determining the Strength of Corrugated Fiberboard*, J. of Composites Technology and Research, Vol. 11, No. 4, pp. 121-127.

[8] Johnson, M. W., and Urbanik, T. J., (1984) *A Nonlinear Theory for Elastic Plates With Application to Characterizing Paper Properties*, J. of Applied Mechanics, Vol. 51, pp 146-152.

[9] Frangopol, D. M., Lee, Y-H., and Williams, K. J., (1996) *Nonlinear Finite Element Reliability Analysis of Concrete*, J. Eng. Mech., Vol. 122, No. 12.

[10] Liu, P-L., and Liu, K-G., (1993) *Selection of Random Field Mesh in Finite Element Reliability Analysis*, J. Eng. Mech., Vol. 119, No. 4.

[11] Liu, P-L., and Der Kiureghian, A., (1991) *Finite Element Reliability of Geometrically Nonlinear Uncertain Structures*, J. Eng. Mech., Vol. 117, No. 8.

[12] Guan, X. L., and Melchers, R. E.., (1999) *A Load Space Formulation for Probabilistic Finite Element Analysis of Structural Reliability*, Probabilistic Engineering Mechanics 14, pp 73-81.

[13] Viadero, F., Bueno, J. I., Lopez de Lacalle, L. N., and Sancibrian R., (1994) *Reliability Computation on Stiffened Plates*, Advances in Engineering Software, **20**, pp 43-48.

[14] Madsen, H. O., Krenk, S., and Lind, N. C., (1986) *Methods of Structural Safety*, Prentice-Hall, New Jersey.

[15] Hasofer, A. M, and Lind, N. C., (1974) *An Exact and Invariant First Order Reliability Format*, Proc. ASCE, J. Eng. Mech. Div., pp 111-121

Paper 1

Buckling of Long Orthotropic Plates Including Higher-Order Transverse Shear

Ulf Nyman and Per Johan Gustafsson
Division of Structural Mechanics
Lund University

Buckling of Long Orthotropic Plates Including Higher-Order Transverse Shear

By Ulf Nyman[1] and Per Johan Gustafsson[2]

ABSTRACT: The problem of buckling of long orthotropic plates under combined in-plane loading is considered. An approximate analytical solution is presented. The concept of a mixed Rayleigh-Ritz method is used considering higher-order shear deformations. The achieved load function of the half buckling wavelength and the inclination of the nodal lines is minimized via a simplex search method. For low transverse shear stiffnesses the model predicts buckling coefficients under in-plane shear load that are of the same order of magnitude as those resulting from a uniaxial compressive load. For a thin plate the critical shear load is larger by 42% compared to the uniaxial case. The model also suggests that for highly anisotropic materials, such as paper, the critical load solution is still influenced by the shear deformation effect at width-to-thickness ratios above 100.

Introduction

The use of paper as a structural member in a packaging environment has inspired research within the field of modeling corrugated panel structures subject to loads of various kinds. Local buckling of corrugated board facings is a limiting design principle of judgement for packages. Examples of work relating to buckling of the facing of a sandwich panel are mentioned in the following. Johnson and Urbanik (1989) analyzed composite plate structures under uniaxial compression and concluded that, in a triangular core sandwich, the facing initiates buckling. Analysis of an aluminum sheet sandwich plate made by Wittrick (1969) showed that buckling modes with inclined nodal lines (where out-of-plane deflection is equal to zero) are possible. Zahn (1973) studied an orthotropic truss core sandwich in axial compression. Anderson (1958) analyzed the instability of isotropic elements of a truss-core sandwich plate. Harris and Auelmann (1960) presented a buckling solution of finite plates subjected to combined in-plane loads using a first-order shear deformation theory. Norris and Kommers (1952) studied sandwich panels under combined loads.

Originally, instability was examined by a number of authors adopting the Kirchoff-Love assumption (thin plate theory). For plates with reasonable thickness or a very large elastic modulus to transverse shear modulus ratio, the buckling load is considerably over-estimated. Therefore, the plane stress assumption is relaxed and transverse shear stresses are considered. Highly anisotropic behavior is found for many fiber based materials, e.g. fiber reinforced composite materials, and for paper, with material stiffness ratios as high

[1]Structural Mechanics, Lund University, PO Box 118, S-221 00 Lund, Sweden.
[2]Structural Mechanics, Lund University, Sweden.

as 600 being reported (Persson 1991), compared to a typical ratio of 2.6 for isotropic materials. Consequently, the need for using refined plate theories including higher-order shear deformations is clear. A number of plate theories based on an assumed displacement field, taking out-of-plane shear effects into account, have been developed. The Reissner-Mindlin (1945) theory allows for deflection independent rotation of the plate cross-section during deformation. Bert and Chang (1972) introduced in the governing differential equations the slope at which the normal forces act on the plate cross section. However, since the theories assume a constant distribution of shear strains through the plate thickness, a correction factor is needed. An improved higher-order theory was presented by Levinson (1980) and Reddy (1984) where the shear stress distribution in the thickness direction follows a parabolic law, vanishing at the plate surfaces.

Exact solutions of some vibration and buckling problems based on the Reddy theory are presented by Reddy and Phan (1985). The buckling solution of the governing differential equations, for a uniaxial load case, is obtained by the Navier solution method. In the present paper the writers propose an approximate method to find the critical load of an orthotropic plate subjected to an arbitrary in-plane combination of homogeneous shear and compression. The solution makes use of a mixed Rayleigh-Ritz variational method in terms of the minimization procedure. In order to find the Ritz coefficients, the parameters associated with unique terms in the energy functional are first solved for in a linear sense. Successively, a load function is minimized with respect to the remaining parameters via a simplex search to find the critical load. The procedure is useful for obtaining a computationally efficient solution of the critical load. In order to solve the critical state, a numerical procedure is necessary for given material properties and load relations. This can easily be programmed by means of standard methods. The result from the critical state analysis can then be used in combination with a numerical method for structural analysis, such as the finite element method.

The obtained approximate solution is a linear interaction model which enables an arbitrary in-plane homogeneous stress state analysis. The solution is compared with numerical results gained from finite element analysis. The agreement is seen to be very good from an engineering point of view. The need for a computationally efficient solution of the critical load is obvious when the structure analyzed contains a large number of potential locations for buckling. An example structure is one made of corrugated core sandwich elements, e.g. Nyman and Gustafsson (1999).

Problem formulation

The analytical approach in the present study is based upon the principle of stationary total potential strain energy. The study here is restricted to infinitely long plates, see Figure 1, such as a structural member of a corrugated medium.

According to the Levinson and Reddy higher-order shear deformation theory, the plate displacement field is given by

$$u = u^0 + z\psi_x - \frac{4z^3}{3h^2}\left(w^0_{,x} + \psi_x\right)$$

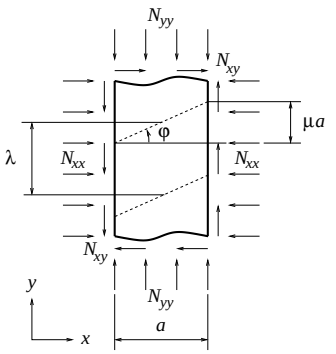

Figure 1: Partial strip of plate.

$$v = v^0 + z\psi_y - \frac{4z^3}{3h^2}\left(w^0_{,y} + \psi_y\right) \qquad (1)$$
$$w = w^0$$

where u^0, v^0 and w^0 are mid-plane displacements, ψ_x, ψ_y are mid-plane cross section rotations about the y-axis and x-axis respectively, and h is the thickness of the plate. Linearly independent displacement coordinate functions ϕ_i, consistent with the chosen boundary conditions, are used to introduce the displacement distributions

$$\psi_i = q_i\phi_i \qquad i = 1, 2, 3 \qquad (2)$$

in which $\psi_1 = w(x, y), \psi_2 = \psi_x(x, y), \psi_3 = \psi_y(x, y)$.

Boundary conditions and coordinate functions

The kinematic boundary conditions of the strip are given by

$$\phi_1(x = 0) = \phi_1(x = a) = 0$$
$$\phi_3(x = 0) = \phi_3(x = a) = 0 \qquad (3)$$

i.e. the strip has zero deflection w and rotation ψ_y at the longitudinal endlines. The nodal lines with zero deflection located in between two half wavelengths (buckling lengths) are assumed to be straight lines: $y = \mu x + p\lambda$ where μ indicates the inclination of the line, λ half the wavelength and $p = 1, 2 \ ... \ \infty$. Transformation of the cross section rotations $\boldsymbol{\phi} = [\phi_2 \ \phi_3]^T$ to the corresponding rotations in a coordinate system rotated counterclockwise $\varphi = \tan^{-1}(\mu)$ and indicated by $\{\ \}'$ is given by

$$\boldsymbol{\phi}' = \mathbf{A}\boldsymbol{\phi} \qquad (4)$$

where the orthogonal transformation matrix $\mathbf{A}$ is given by

$$\mathbf{A} = \begin{bmatrix} \cos(\varphi) & \sin(\varphi) \\ -\sin(\varphi) & \cos(\varphi) \end{bmatrix} \qquad (5)$$

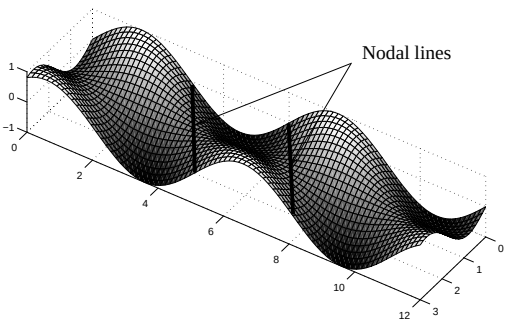

Figure 2: Transformed rotation coordinate function ϕ_2'.

Then, the boundary conditions of the joint edges of two half wavelengths in the y-direction are

$$\begin{aligned} &\phi_1(y=\mu x)=\phi_1(y=\mu x+p\lambda)=0 \\ &\phi_2'(y=\mu x)=\phi_2'(y=\mu x+p\lambda)=0 \qquad p=1,2,3\ldots\infty \end{aligned} \tag{6}$$

i.e. periodic. Since the deflection derivative $\partial w/\partial x'$ is zero along the nodal lines, zero cross section rotation ψ_x' corresponds to zero shear stress σ_{13}'.

The cross section rotation distributions are assumed to have the same form as the deflection derivative, see Harris and Auelmann (1960), i.e. $\phi_2 \sim w^0_{,x}, \phi_3 \sim w^0_{,y}$. Then the present choice of coordinate functions ϕ_i is

$$\begin{bmatrix} \phi_1 \\ \phi_2 \\ \phi_3 \end{bmatrix} = \begin{bmatrix} \mathrm{Im}\, e^{i\frac{\pi}{a}x}\mathrm{Im}\, e^{i[\frac{\pi}{\lambda}(y-p(x))]} \\ \frac{1}{a}\mathrm{Re}\, e^{i\frac{\pi}{a}x}\mathrm{Im}\, e^{i[\frac{\pi}{\lambda}(y-p(x))]} - \frac{\mu}{\lambda}\mathrm{Im}\, e^{i\frac{\pi}{a}x}\mathrm{Re}\, e^{i[\frac{\pi}{\lambda}(y-p(x))]} \\ \mathrm{Im}\, e^{i\frac{\pi}{a}x}\mathrm{Re}\, e^{i[\frac{\pi}{\lambda}(y-p(x))]} \end{bmatrix} \tag{7}$$

In Figure 2 the transformed rotation coordinate function ϕ_2' is plotted over the plate domain.

Constitutive relations

The elastic orthotropic constitutive behavior is described by the stress-strain relation

$$\boldsymbol{\sigma} = \mathbf{D}\boldsymbol{\varepsilon} \tag{8}$$

or

$$\begin{bmatrix} \sigma_{11} \\ \sigma_{22} \\ \sigma_{12} \\ \sigma_{13} \\ \sigma_{23} \end{bmatrix} = \begin{bmatrix} D_{11} & D_{12} & D_{14} & D_{15} & D_{16} \\ & D_{22} & D_{24} & D_{25} & D_{26} \\ & & D_{44} & D_{45} & D_{46} \\ & sym. & & D_{55} & D_{56} \\ & & & & D_{66} \end{bmatrix} \begin{bmatrix} \varepsilon_{11} \\ \varepsilon_{22} \\ \gamma_{12} \\ \gamma_{13} \\ \gamma_{23} \end{bmatrix} \tag{9}$$

with

$$
\begin{aligned}
&D_{14} = D_{15} = D_{16} = D_{24} = D_{25} = D_{26} = D_{45} = D_{46} = D_{56} = 0 \\
&D_{11} = \frac{E_{11}}{1-\nu_{12}\nu_{21}},\ D_{12} = \frac{\nu_{21}E_{11}}{1-\nu_{12}\nu_{21}},\ D_{22} = \frac{E_{22}}{1-\nu_{12}\nu_{21}} \\
&D_{44} = G_{12},\ D_{55} = G_{13},\ D_{66} = G_{23}
\end{aligned} \tag{10}
$$

where E, G and ν are material constants. It is here assumed that the material axes coincide with the coordinate axes of the plate. The kinematic relations are obtained by applying the small strain tensor format on (1)

$$
\begin{aligned}
\boldsymbol{\varepsilon} = \begin{bmatrix} \varepsilon_{11} \\ \varepsilon_{22} \\ \gamma_{12} \\ \gamma_{13} \\ \gamma_{23} \end{bmatrix} = \begin{bmatrix} u_{,x} \\ v_{,y} \\ v_{,x} + u_{,y} \\ w_{,x} + \psi_x \\ w_{,y} + \psi_y \end{bmatrix} + z \begin{bmatrix} \psi_{x,x} \\ \psi_{y,y} \\ \psi_{y,x} + \psi_{x,y} \\ 0 \\ 0 \end{bmatrix} \\
-\tfrac{4z^2}{h^2} \begin{bmatrix} 0 \\ 0 \\ 0 \\ w_{,x} + \psi_x \\ w_{,y} + \psi_y \end{bmatrix} - \tfrac{4z^3}{3h^3} \begin{bmatrix} w_{,xx} + \psi_{x,x} \\ w_{,yy} + \psi_{y,y} \\ \psi_{y,x} + \psi_{x,y} + 2w_{,xy} \\ 0 \\ 0 \end{bmatrix}
\end{aligned} \tag{11}
$$

Variational formulation

By defining the initial in-plane loading vector $\mathbf{N}$ for the plate

$$
\mathbf{N} = \begin{bmatrix} N_{11} \\ N_{12} \\ N_{22} \end{bmatrix} \tag{12}
$$

the energy varying during buckling can be obtained, e.g. Bazant (1991), by integrating over the plate region

$$
U_1 = \frac{1}{2}\int\int_A N_{ij} w_{,i} w_{,j} dA \qquad i,j = 1,2 \tag{13}
$$

$$
U_2 = -\frac{1}{2}\int\int\int_V \sigma_{ij}\varepsilon_{ij} dV = -\frac{1}{2}\int\int\int_V \left[D_{11}\varepsilon_{11}^2 + 2D_{12}\varepsilon_{11}\varepsilon_{22} + D_{22}\varepsilon_{22}^2 + D_{44}\gamma_{12}^2\right] dV \qquad i,j = 1,2 \tag{14}
$$

$$
U_3 = -\frac{1}{2}\int\int\int_V G_{ij}\gamma_{ij}\gamma_{ij} dV \qquad i = 1,2;\ j = 3 \tag{15}
$$

where U_1 is the pre-strain energy, U_2 is due to the in-plane stress and U_3 is due to the out-of-plane shear energy. To capture the correct integration of strain energy beyond the plate mid-plane, consideration must be given to the strain variation over the thickness h. In doing so, integration is done over the plate volume. The expressions (14) and (15) can be reduced to area integrals obtaining expressions in terms of the displacement

distribution functions. If (2) is substituted in (11) and integration of (14) and (15) is performed over the plate thickness $-h/2..h/2$, the following is obtained

$$U_2 = -\frac{1}{2}\int\int_A \frac{D_{ij}h^3}{315}\left(\frac{5}{4}w_{,ii}w_{,jj} - 4w_{,ii}\psi_{j,j} - 4w_{,jj}\psi_{i,i} + 17\psi_{i,i}\psi_{j,j}\right) + \frac{D_{kk}h^3}{315}(1-\delta_{ij})\left(\frac{5}{2}w_{,ij}w_{,ji} - 16w_{,ij}\psi_{i,j} + 17\psi_{i,j}\psi_{j,i} + 17\psi_{i,j}\psi_{i,j}\right)dA \qquad i,j = 1,2;\ k = 4 \tag{16}$$

$$U_3 = -\frac{1}{2}\int\int_A \frac{8h}{15}G_{ij}\left(w_{,i} + \psi_i\right)^2 dA \qquad i = 1,2;\ j = 3 \tag{17}$$

where δ_{ij} is the Kronecker delta function.

The equilibrium condition of the plate can be expressed by a stationary first variation of energy. According to (13), (16) and (17) this is expressed as

$$\delta\Pi = 0 \quad \rightarrow \quad \frac{\partial\Pi}{\partial q_i} = 0 \quad i = 1,2,3, \tag{18}$$

Π being defined as the energy functional $\Pi = U_1 + U_2 + U_3$.

Sectional moments

The section quantity $\tilde{M}_{ij}$ is obtained by the definition

$$\tilde{M}_{ij} = \int_{-h/2}^{h/2} \sigma_{ij} z dz \qquad i,j = 1,2 \tag{19}$$

which yields the constitutive relations in terms of the plate

$$\tilde{M}_{ij} = \tilde{D}_{ij}\kappa_{ij}^D \tag{20}$$

where the flexural stiffness $\tilde{D}_{ij}$ is given by

$$\begin{bmatrix} \tilde{D}_{11} \\ \tilde{D}_{12} \\ \tilde{D}_{22} \end{bmatrix} = \frac{h^3}{12(1-\nu_{12}\nu_{21})}\begin{bmatrix} E_{11} \\ E_{12} \\ E_{22} \end{bmatrix} \tag{21}$$

and the bending deformation κ_{ij}^D

$$\begin{bmatrix} \kappa_{11}^D \\ \kappa_{12}^D \\ \kappa_{22}^D \end{bmatrix} = \frac{1}{5}\begin{bmatrix} w_{,11} - 4\psi_{1,1} + \nu_{21}(w_{,22} - 4\psi_{2,2}) \\ 2w_{,12} - 4(\psi_{2,1} + \psi_{1,2}) \\ \nu_{12}(w_{,11} - 4\psi_{1,1}) + w_{,22} - 4\psi_{2,2} \end{bmatrix} \tag{22}$$

Note that the tilde operator is used on $\tilde{M}_{ij}$ in order not to be confused with the stress resultant M_i given by Reddy (1984).

Resultant moments at the boundary

By recalling the transformation matrix given by (5), the section moments (20) transform according to

$$\tilde{\mathbf{M}}' = \mathbf{A}\tilde{\mathbf{M}}\mathbf{A}^T \tag{23}$$

The resulting moments $\tilde{M}_{11}$ and $\tilde{M}'_{22}$, upon the tranformation (23),

$$\begin{aligned} &\tilde{M}_{11}(x=0) = \tilde{M}_{11}(x=a) \\ &\tilde{M}'_{22}(y=\mu x) = \tilde{M}'_{22}(y=\mu x + p\lambda) \qquad p = 1,2,3 \ldots \infty \end{aligned} \tag{24}$$

can be obtained from (20)-(22) and (2). It is concluded (calculations not shown here) that section moments develop, symmetrically distributed around the edge midpoints, with zero average value. This is due to the coordinate functions, inferring an approximate displacement field. The moments are proportional to the inclination of the nodal lines; thus the approximation disappears for the simply supported case when no shear load is present.

Buckling solution

In order to find the complete solution, the energy functional in (18) should be minimized with respect to both q_i and λ, μ. This produces a set of equations in q_i and λ, μ which are not linear. However, a non-linear equation system is undesirable since a numerical procedure required to find the critical solution would involve producing initial guess values. This is straightforward for λ and μ, whereas q_i are of more arbitrary form, making it difficult to find an automated solution process. Therefore the solution strategy chosen is first solving for q_i in a linear sense, and then using this solution to find the parameters λ and μ.

The expression for Π can be determined by evaluating (13), (16) and (17) for the given set of displacement functions. By then applying (18) on Π the following homogeneous equation system is obtained

$$\frac{\partial \Pi}{\partial q_j} = B_{ij} q_j = 0 \qquad i,j = 1,2,3 \tag{25}$$

with the coefficients

$$\begin{aligned} B_{11} &= -\frac{c_1}{5040a^3h^2\lambda^3}\Big[-5D_{11}c_1c_3h - 10a^2c_1c_2h(D_{12}+2D_{44}) - 5D_{22}a^4c_1h \\ &\quad -672a^2h\lambda^2(D_{55}c_2 + D_{66}a^2) + 1260a^2\lambda^2(N_{11}c_2 + 2N_{12}a^2\mu + N_{22}a^2)\Big] \\ B_{12} &= \frac{\pi h}{315a^3\lambda^3}\Big[-D_{11}c_1c_3 - a^2c_1c_2(D_{12}+2D_{44}) + 42D_{55}a^2c_2\lambda^2\Big] \\ B_{13} &= -\frac{\pi h}{315a\lambda^2}\Big[c_1c_2(D_{12}+2D_{44}) + D_{22}a^2c_1 - 42D_{66}a^2\lambda^2\Big] \\ B_{22} &= \frac{h}{1260a^3\lambda^3}\Big[17D_{11}c_1c_3 + 17D_{44}a^2c_1c_2 + 168D_{55}a^2c_2\lambda^2\Big] \end{aligned}$$

$$
\begin{aligned}
B_{23} &= \frac{17c_1c_2h}{1260a\lambda^2}(D_{12}+D_{44}) \\
B_{33} &= \frac{h}{1260a\lambda^3}\left[17D_{44}c_1(4a^4\mu^4-5a^2c_2\mu^2-c_3)\right. \\
&\quad \left.+17D_{22}a^2c_1(c_2-a^2\mu^2)+168D_{66}a^2\lambda^4)\right] \\
B_{21} &= B_{12},\ B_{31}=B_{13},\ B_{32}=B_{23} \\
c_1 &= \pi^2h^2,\ c_2=\lambda^2+a^2\mu^2,\ c_3=\lambda^4+6a^2\lambda^2\mu^2+a^4\mu^4
\end{aligned} \tag{26}
$$

By observing that B_{ij} in (25) is symmetric the following holds

$$
\frac{\partial^2\Pi}{\partial q_i\partial q_j}=\frac{\partial^2\Pi}{\partial q_j\partial q_i} \tag{27}
$$

and the symmetric property of the stiffness matrix is fulfilled, i.e. the system is conservative; see Bazant (1991) for a more thorough discussion of this subject. The critical state of (25) is given by the singularity condition on B_{ij}, i.e. $\det(B_{ij})=0$. Applying this and using the parameterization

$$
\mathbf{N}=\begin{bmatrix} N_{11} \\ N_{12} \\ N_{22} \end{bmatrix}=\hat{N}\begin{bmatrix} \alpha \\ \beta \\ \chi \end{bmatrix} \tag{28}
$$

the critical stress state is expressed by the load function

$$
\hat{N}(\lambda,\mu)=\frac{G}{60a^2\lambda^2\left(c_2\alpha+2a^2\beta\mu+a^2\chi\right)H} \tag{29}
$$

where

$$
G=\sum_{i=1}^{33}g_i \qquad H=\sum_{i=1}^{27}h_i \tag{30}
$$

The coefficients g_i and h_i are given in Appendix III.

The minimum of $\hat{N}$, $\hat{N}_{cr}$, is now exclusively determined by the parameters $\bar{x}=(\lambda/a,\mu)$, which are determined by a numerical minimization procedure. The procedure can be described by

1. Use starting values of $\bar{x}_0=(\lambda_0/a,\mu_0)$. The appropriate ranges of these values are $1/2\le\lambda_0/a\le 2$ and $0\le\mu_0\le 2$.

2. Evaluate with the current value of $\bar{x}$ the objective function $\hat{N}=\hat{N}(\bar{x})$. Determine the new values of $\bar{x}$ in terms of the Nelder-Mead simplex method.

3. Repeat step 2 until the termination tolerance is reached. The termination tolerance can be specified for either $\bar{x}$ or $\hat{N}(\bar{x})$.

4. The final value of $\bar{x}=\bar{x}_{cr}$ will yield the critical stress state $\hat{N}=\hat{N}_{cr}$.

The appropriate range of the starting values $\bar{x}_0$ will depend on the degree of orthotropy, and on the load condition. For the load cases studied here, numerical experience shows that choosing the lower limit $\bar{x}_0=(1/2,0)$ and the upper limit $\bar{x}_0=(2,2)$ is sufficient in order to find the critical solution $\bar{x}_{cr}$.

Table 1: Nondimensionalized buckling coefficients for the isotropic material.

β	$\bar{x}^a$	$\hat{K}^a$	$\bar{x}^b$	$\hat{K}^b$	$\bar{x}^c$	$\hat{K}^c$
0	(0.993,0)	3.944	(1.281,0)	3.797	(16.815,0)	2.979
0.2	(0.998,0.099)	4.641	(1.279,0.096)	4.366	(7.205,0.08)	3.375
0.4	(1.01,0.188)	5.137	(1.274,0.184)	4.796	(4.034,0.157)	3.759
0.6	(1.025,0.262)	5.455	(1.267,0.257)	5.097	(2.909,0.227)	4.107
1	(1.056,0.369)	5.764	(1.255,0.365)	5.437	(2.073,0.339)	4.639
3	(1.135,0.564)	5.866	(1.23,0.563)	5.714	(1.43,0.556)	5.422
5	(1.162,0.619)	5.788	(1.223,0.618)	5.696	(1.335,0.616)	5.531
10	(1.185,0.664)	5.69	(1.217,0.664)	5.644	(1.271,0.663)	5.569
100	(1.208,0.707)	5.565	(1.212,0.707)	5.56	(1.217,0.707)	5.554

[a] $\alpha = 0, \chi = 1$
[b] $\alpha = 0.2, \chi = 1$
[c] $\alpha = 0.5, \chi = 1$

Numerical results for three materials

In the following, numerical results are presented for the case of three material constitutions under various load conditions. First, an isotropic material is considered, i.e. $\nu_{12} = \nu_{21} = 0.3$. Second, an orthotropic material with stiffness ratios $E_{11}/E_{22} = 2$, $E_{11}/G_{12} = 3$, $E_{11}/G_{13} = E_{11}/G_{23} = 30$ and $\nu_{12} = 0.2$ is considered. Finally, an orthotropic material, typical of corrugated board constituents, is examined. This last material has the same stiffness properties as the second material except that $E_{11}/G_{13} = 300$. The value of E_{11} is taken to be $E_{11} = 7$ GPa and $a = 7\text{mm}, h = a/20$ for all materials. A non-dimensionalized buckling coefficient is computed according to

$$\hat{K} = \frac{a^2 \hat{N}_{cr}}{\pi^2 \tilde{D}_{11}} (\alpha + \beta + \chi) \tag{31}$$

The termination tolerance used for the simplex search is 1×10^{-8} and 1×10^{-4} for $\bar{x}$ and $\hat{N}$, respectively. The results are presented in Tables 1, 2 and 3.

In addition, the influence of varying plate thickness is examined for the three materials. The results from this analysis are presented in Tables 4, 5 and 6.

In Table 1 it is seen that for $\alpha = \beta = 0, \chi = 1$, i.e. uniaxial load in the y-direction, the ratio of the half buckling wavelength to plate width λ/a is close to unity and the buckling coefficient is slightly lower than the classical plate solution $K = 4.0$. It should be pointed out that the load case $\beta = 0$, i.e. a biaxial load case, provides the exact solution as the displacement distribution functions in the present model have the same form as in Reddy and Phan (1985). Therefore, the top line values in Tables 1, 2 and 3 correspond to the exact solution of a long plate. As the shear stress increases, the inclination of the nodal line converges to $1/\sqrt{2}$, which is valid for a similar analytical analysis[3] of isotropic

[3] Nodal lines considered as straight.

Table 2: Nondimensionalized buckling coefficients for an orthotropic material, no. 2.

β	$\bar{x}^a$	$\hat{K}^a$	$\bar{x}^b$	$\hat{K}^b$	$\bar{x}^c$	$\hat{K}^b$
0	(0.795,0)	2.572	(1.059,0)	2.689	(2.263,0)	2.438
0.2	(0.798,0.078)	3.039	(1.056,0.076)	3.068	(2.166,0.067)	2.734
0.4	(0.804,0.151)	3.397	(1.048,0.147)	3.368	(1.956,0.131)	3.004
0.6	(0.813,0.214)	3.65	(1.038,0.21)	3.59	(1.746,0.191)	3.238
1	(0.831,0.312)	3.934	(1.018,0.307)	3.861	(1.458,0.288)	3.583
3	(0.883,0.504)	4.145	(0.972,0.503)	4.116	(1.093,0.498)	4.043
5	(0.902,0.56)	4.124	(0.959,0.56)	4.111	(1.027,0.558)	4.079
10	(0.919,0.607)	4.079	(0.949,0.607)	4.075	(0.981,0.607)	4.066
100	(0.936,0.652)	4.011	(0.939,0.652)	4.011	(0.942,0.652)	4.011

[a] $\alpha = 0, \chi = 1$
[b] $\alpha = 0.3, \chi = 1$
[c] $\alpha = 0.6, \chi = 1$

thin plates, e.g. Timoshenko and Gere (1961). As the stress in the x-direction increases, the half buckling wavelength will become infinitely large and the the buckling problem is similar to that of a hinged column member. However, it is obvious that for very large shear stresses the influence of the normal stresses has little significance. This load condition corresponds to the bottom row in Table 1.

In Table 2 the orthotropic material no. 2 is used. The transverse stiffness is reduced to 1/30 that of the Young's modulus in the x-direction. The value of λ/a in Table 2 is seen to decrease with decreasing transverse stiffness. As the shear load increases, the half buckling wavelength increases. It is seen that the final value of μ corresponding to $\beta = 100$ is lower than for the isotropic material.

The results from material no. 3 are presented in Table 3. The lowered transverse shear stiffness in the xz-plane results in a reduced buckling coefficient, for the case $\alpha = \beta = 0$ and $\chi = 1$, by 32% compared to material no. 2. The same comparison between materials no. 1 and no. 3 shows a reduced buckling coefficient of 56%. The value of μ when $\alpha = 0$ and $\beta = 100$, i.e. close to pure shear, for this material is larger than for both the isotropic material and material no. 2. This indicates that a low transverse shear stiffness will increase the inclination of the nodal lines. It is remarkable to note that for the case $\alpha = 0, \beta = 100$ the buckling coefficient is almost equal that of the pure uniaxial compression case $\alpha = \beta = 0$. This was not the case for the previously examined materials which showed an increased shear buckling coefficient. Both the orthotropic materials show less sensitivity to load in the x-direction in the sense of the solution of λ. In Tables 2 and 3, the last two columns represent the solution for the case $\alpha = 0.6, \chi = 1$. The isotropic material can only be analyzed until $\alpha = 0.5$ before λ becomes very large.

As a comparison with finite element results (Nyman and Gustafsson 1999), the values of $\hat{K}^a$ from Table 3 are plotted[4] in Figure 3. It should be noted that the circles in Figure

[4] HSDPT – Higher-order shear deformation plate theory.

Table 3: Nondimensionalized buckling coefficients for an orthotropic material, no. 3.

β	$\bar{x}^a$	$\hat{K}^a$	$\bar{x}^b$	$\hat{K}^b$	$\bar{x}^c$	$\hat{K}^c$
0	(0.867,0)	1.751	(1.179,0)	1.761	(3.477,0)	1.519
0.2	(0.868,0.179)	2.03	(1.158,0.175)	1.984	(2.945,0.12)	1.704
0.4	(0.873,0.341)	2.165	(1.112,0.35)	2.104	(2.172,0.25)	1.864
0.6	(0.882,0.469)	2.204	(1.075,0.497)	2.144	(1.639,0.41)	1.976
1	(0.903,0.634)	2.177	(1.042,0.677)	2.128	(1.259,0.685)	2.036
3	(0.949,0.89)	1.973	(1.009,0.917)	1.959	(1.075,0.942)	1.938
5	(0.963,0.954)	1.892	(1.001,0.972)	1.886	(1.041,0.99)	1.877
10	(0.974,1.005)	1.818	(0.994,1.015)	1.817	(1.015,1.025)	1.814
100	(0.985,1.054)	1.742	(0.988,1.055)	1.742	(0.99,1.056)	1.742

[a] $\alpha = 0, \chi = 1$
[b] $\alpha = 0.3, \chi = 1$
[c] $\alpha = 0.6, \chi = 1$

Table 4: Influence of thickness for the isotropic material.

a/h	$\hat{K}^d$	$\hat{K}^e$	$\hat{K}^f$
5	3.232	4.589	4.207
10	3.784	5.499	5.254
40	3.986	5.833	5.646
80	3.996	5.851	5.666
100	3.998	5.853	5.669
500	4	5.856	5.673

Table 5: Influence of thickness for material no. 2.

a/h	$\hat{K}^d$	$\hat{K}^e$	$\hat{K}^f$
5	0.831	1.088	0.928
10	1.859	2.671	2.457
40	2.826	4.391	4.633
80	2.897	4.517	4.808
100	2.905	4.533	4.829
500	2.92	4.559	4.866

Table 6: Influence of thickness for material no. 3.

a/h	$\hat{K}^d$	$\hat{K}^e$	$\hat{K}^f$
5	0.508	0.497	0.345
10	1.01	1.069	0.771
40	2.443	3.546	3.309
80	2.778	4.26	4.379
100	2.827	4.364	4.546
500	2.917	4.552	4.854

3 are obtained from a numerical minimization of the parameters λ and μ, in the finite element procedure. In addition, the value of the buckling coefficient when neglecting the transverse shear, a material with large transverse shear modulus is studied, see the upper solid line in Figure 3. It is seen that the difference between considering and not considering the transverse shear is large for all of the analyzed load combinations.

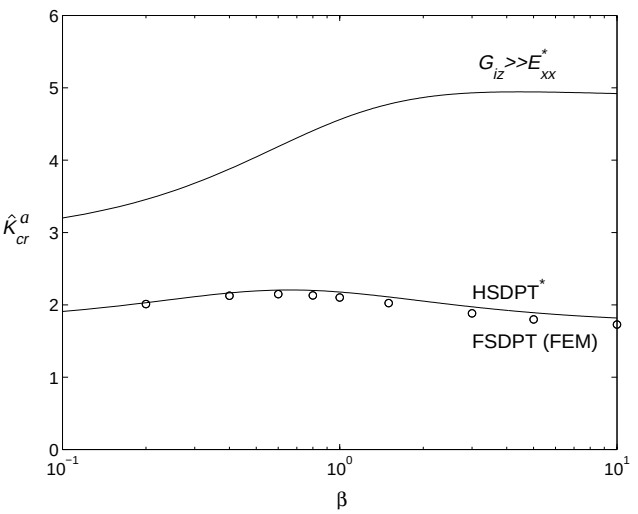

Figure 3: Buckling coefficient with increasing shear load. *Present model.

In Tables 4, 5 and 6 the superscripts d, e and f refer to $\alpha = \beta = 0, \chi = 1$ and $\alpha = 0, \beta = 1, \chi = 1$ and $\alpha = 0, \beta = 100, \chi = 1$, respectively. The results in Table 4 show that for the purely uniaxial load case the critical load converges to the thin plate solution between $10 < a/h < 40$. The same holds for the case of shear load, $\alpha = 0, \beta = 100, \chi = 1$. It is well-known that for isotropic plates, the critical load is fairly close to that of the thin plate solution when the width-to-thickness ratio is ~ 20. For material no. 2, Table 5, the

FSDPT – First-order shear deformation plate theory.

value of the buckling coefficient levels out at $a/h = 80$. For material no. 3 the buckling coefficient has not yet reached a stable level at $a/h = 100$. In Figure 4 the results from Tables 4-6 are also plotted. The figure suggests that for highly anisotropic materials, the critical load solution is still influenced by the shear deformation effect at width-to-thickness ratios above 100. It is expected that the influence is even more significant if the transverse stiffness in the yz-plane is very low, i.e. the same order as G_{13}.

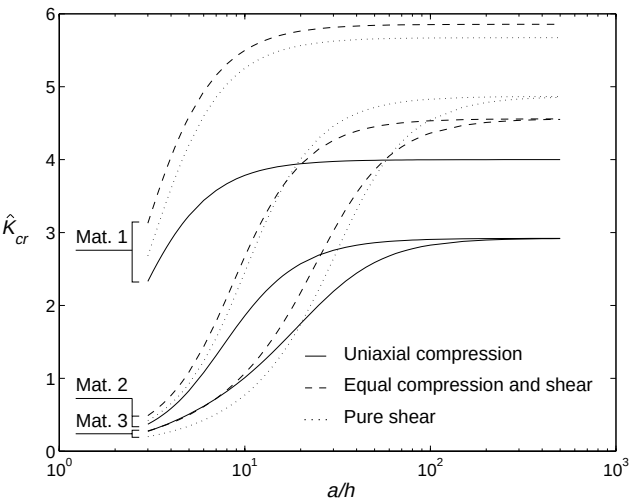

Figure 4: Buckling coefficient with increasing width-to-thickness ratio.

Concluding remarks

An approximate analytical buckling solution of long orthotropic plates under combined in-plane load is presented. A higher-order shear deformation theory is used for the plate displacement field. The solution makes use of a mixed Rayleigh-Ritz variational statement. The Ritz displacement coordinate functions are simple, one-term approximations of the displacement field. The achieved load function of the half buckling wavelength and the inclination of the nodal lines is minimized via a simplex search method.

For low transverse shear stiffnesses the model predicts buckling coefficients under in-plane shear load that are of the same order of magnitude as those resulting from a uniaxial compressive load. For a thin plate the critical shear load is larger by 42% compared to the uniaxial case. The model also suggests that that for highly anisotropic materials, the critical load solution is still influenced by the shear deformation effect at width-to-thickness ratios above 100.

For the analysis cases studied in this paper the present model provides an economic way of performing parameter studies on materials with different stiffness properties subject to various load conditions.

Acknowledgements

This work was supported by "Bo Rydins stiftelse för vetenskaplig forskning" [The Bo Rydin Foundation for Scientific Research] and by FPIRC - Forest Products Industry Research College.

Appendix

References

[1] Anderson, M. S. (1958). "Local Instability of the Elements of a Truss-Core Sandwich Plate." *NACA Tech.,* Note 4292.

[2] Bazant, Z. P. (1991). "Stability of Structures." *Oxford University Press.*

[3] Bert, C. W., and Chang, S. (1972). "Shear-Flexible Orthotropic Plates Loaded In Plane." *J. Eng. Mech. Division,* Vol. 98, No. EM6, 1499-1509.

[4] Harris, L. A., and Auelmann, R. A. (1960). "Stability of flat simply-supported, corrugated-core sandwich plates under combined loads." *J. Aero/Space Sci.,* **27**, 7, 525-534.

[5] Johnson, M. W., and Urbanik, T. J. (1989). "Analysis of the Localized Buckling in Composite Plate Structures with application to Determining the Strength of Corrugated Fiberboard." *J. of Composites Technology and Research,* Vol. 11, No. 4, 121-127.

[6] Levinson, M. (1980). "An Accurate Simple Theory of the Statics and Dynamics of Elastic Plates." *Mech. Res. Communications,* 7, 343-350.

[7] Norris, C. B., and Kommers, W. J. (1952). "Critical loads of a rectangular, flat sandwich panel subjected to two direct loads combined with a shear load." FPL Report 1833.

[8] Nyman, U., and Gustafsson, P. J. (1999). "Local buckling of corrugated board facings." *Proceedings of the European Conference on Computational Mechanics,* Munich, Germany.

[9] Persson, K. (1991). "Material Model for Paper: Experimental and Theoretical Aspects." Diploma Report, Lund University, Sweden.

[10] Reddy, J. N. (1984). "A Simple Higher-Order Theory for Laminated Composite Plates." *J. Appl. Mech.,* 51(4), 745-752.

[11] Reddy, J. N., and Phan, N. D. (1985). "Stability and Vibration of Isotropic, Orthotropic and Laminated Plates According to a Higher-Order Shear Deformation Theory." *J. of Sound and Vibration,* **98**(2), 157-170.

[12] Reissner, E. (1945). "The Effect of Transverse Shear Deformation on the Bending of Elastic Plates." *J. Appl. Mech.,* 12, A69-A77.

[13] Seide, P. (1961). "Comments on: Stability of flat simply-supported, corrugated-core sandwich plates under combined loads." *J. Aerospace Sci.,* **28**, 3, 248.

[14] Timoshenko, S. P., and Gere, J. M. (1961). "Theory of Elastic Stability." *McGraw-Hill.*

[15] Wittrick, W. H., and Curzon, P. L. V. (1969). "Buckling of a Series of Equidistant Longitudinal Supports in Combined Longitudinal Compression and Shear." *The Aeronautical Quarterly.*

[16] Wittrick, W. H., and Curzon, P. L. V. (1969). "Nodal Lines for Long Plates in Combined Shear and Compression with Sinusoidal Edge Rotations." *The Aeronautical Quarterly*

[17] Zahn, J. J. (1973). "Local Buckling of Orthotropic Truss-Core Sandwich." Research paper, USDA Forest Service.

Notation

$\mathbf{A}$ =Transformation matrix
D_{ij} =Stiffness matrix coefficients
$\tilde{D}_{ij}$ =Flexural stiffness
E_{ij} =Young's Modulus of Elasticity
G_{ij} =Shear Modulus
$\hat{K}$ =Nondimensionalized buckling coefficient
$\tilde{M}_{ij}$ =Section moment
$\mathbf{N}$ =In plane stress matrix
$\hat{N}$ =Parameterized critical stress
$\hat{N}_{cr}$ =Minimum critical stress
U_1 =Pre-strain energy
U_2 =In-plane normal strain energy
U_3 =Out-of-plane shear strain energy
a =Plate width
b =Plate length
h =Plate thickness
q_i =Amplitude functions
(u, v, w) =Plate displacement field
$\bar{x}$ =Vector of shape factors λ and μ
Π =Potential elastic energy
(α, β, χ) =Load parameters
δ =Variational operator
δ_{ij} =Kronecker delta function
ε_{ij} =Elastic strain tensor

ϕ_i =Displacement coordinate functions
κ_{ij}^D =Bending deformation
λ =Half buckling wavelength
μ =Inclination of nodal lines
ν_{ij} =Poisson's ratio
ψ_i =Displacement distribution functions
ψ_x, ψ_y =Cross section rotations
$\{\ \}_{,i}$ =Partial derivative with respect to coordinate i
$\{\ \}'$ =Transformed quantity
$\{\ \}^T$ =Transpose of matrix

Fraction coefficients

$$
\begin{aligned}
&g_1 = 17\pi^6 c_3^2 D_{11}^2 D_{22} a^2 h^7 \quad g_2 = 17\pi^6 c_2 c_3^2 D_{11}^2 D_{44} h^7 \\
&g_3 = 168\pi^4 c_3^2 D_{11}^2 D_{66} a^2 h^5 \lambda^2 \quad g_4 = -17\pi^6 c_3 c_2^2 D_{11} D_{12}^2 a^2 h^7 \\
&g_5 = 34\pi^6 c_2 c_3 D_{11} D_{12} D_{22} a^4 h^7 \quad g_6 = 336\pi^4 c_2 c_3 D_{11} D_{12} D_{66} a^4 h^5 \lambda^2 \\
&g_7 = 17\pi^6 c_3 D_{11} D_{22}^2 a^6 h^7 \quad g_8 = 102\pi^6 c_2 c_3 D_{11} D_{22} D_{44} a^4 h^7 \\
&g_9 = 14280\pi^4 c_2 c_3 D_{11} D_{22} D_{55} a^4 h^5 \lambda^2 \quad g_{10} = 14280\pi^4 c_3 D_{11} D_{22} D_{66} a^6 h^5 \lambda^2 \\
&g_{11} = 68\pi^6 c_3 c_2^2 D_{11} D_{44}^2 a^2 h^7 \quad g_{12} = 14280\pi^4 c_3 c_2^2 D_{11} D_{44} D_{55} a^2 h^5 \lambda^2 \\
&g_{13} = 14952\pi^4 c_2 c_3 D_{11} D_{44} D_{66} a^4 h^5 \lambda^2 \\
&g_{14} = 141120\pi^2 c_2 c_3 D_{11} D_{55} D_{66} a^4 h^3 \lambda^4 \\
&g_{15} = -34\pi^6 c_2^3 D_{12}^3 a^4 h^7 \quad g_{16} = -17\pi^6 c_2^2 D_{12}^2 D_{22} a^6 h^7 \\
&g_{17} = -136\pi^6 c_2^3 D_{12}^2 D_{44} a^4 h^7 \quad g_{18} = -14112\pi^4 c_2^3 D_{12}^2 D_{55} a^4 h^5 \lambda^2 \\
&g_{19} = -14112\pi^4 c_2^2 D_{12}^2 D_{66} a^6 h^5 \lambda^2 \quad g_{20} = 336\pi^4 c_2^2 D_{12} D_{22} D_{55} a^6 h^5 \lambda^2 \\
&g_{21} = -136\pi^6 c_2^3 D_{12} D_{44}^2 a^4 h^7 \quad g_{22} = -27888\pi^4 c_2^3 D_{12} D_{44} D_{55} a^4 h^5 \lambda^2 \\
&g_{23} = -27888\pi^4 c_2^2 D_{12} D_{44} D_{66} a^6 h^5 \lambda^2 \quad g_{24} = 282240\pi^2 c_2^2 D_{12} D_{55} D_{66} a^6 h^3 \lambda^4 \\
&g_{25} = 17\pi^6 c_2 D_{22}^2 D_{44} a^8 h^7 \quad g_{26} = 168\pi^4 c_2 D_{22}^2 D_{55} a^8 h^5 \lambda^2 \\
&g_{27} = 68\pi^6 c_2^2 D_{22} D_{44}^2 a^6 h^7 \quad g_{28} = 14952\pi^4 c_2^2 D_{22} D_{44} D_{55} a^6 h^5 \lambda^2 \\
&g_{29} = 14280\pi^4 c_2 D_{22} D_{44} D_{66} a^8 h^5 \lambda^2 \quad g_{30} = 141120\pi^2 c_2 D_{22} D_{55} D_{66} a^8 h^3 \lambda^4 \\
&g_{31} = 672\pi^4 c_2^3 D_{44}^2 D_{55} a^4 h^5 \lambda^2 \quad g_{32} = 672\pi^4 c_2^2 D_{44}^2 D_{66} a^6 h^5 \lambda^2 \\
&g_{33} = 564480\pi^2 c_2^2 D_{44} D_{55} D_{66} a^6 h^3 \lambda^4
\end{aligned}
\tag{32}
$$

$$
\begin{aligned}
&h_1 = 289\pi^4 D_{11} D_{22} a^6 h^4 \mu^4 \quad h_2 = 1734\pi^4 D_{11} D_{22} a^4 h^4 \lambda^2 \mu^2 \\
&h_3 = 289\pi^4 D_{11} D_{22} a^2 h^4 \lambda^4 \quad h_4 = 289\pi^4 D_{11} D_{44} a^6 h^4 \mu^6 \\
&h_5 = 2023\pi^4 D_{11} D_{44} a^4 h^4 \lambda^2 \mu^4 \quad h_6 = 2023\pi^4 D_{11} D_{44} a^2 h^4 \lambda^4 \mu^2 \\
&h_7 = 289\pi^4 D_{11} D_{44} h^4 \lambda^6 \quad h_8 = 2856\pi^2 D_{11} D_{66} a^6 h^2 \lambda^2 \mu^4 \\
&h_9 = 17136\pi^2 D_{11} D_{66} a^4 h^2 \lambda^4 \mu^2 \quad h_{10} = 2856\pi^2 D_{11} D_{66} a^2 h^2 \lambda^6 \\
&h_{11} = -289\pi^4 D_{12}^2 a^6 h^4 \mu^4 \quad h_{12} = -578\pi^4 D_{12}^2 a^4 h^4 \lambda^2 \mu^2 \\
&h_{13} = -289\pi^4 D_{12}^2 a^2 h^4 \lambda^4 \quad h_{14} = -578\pi^4 D_{12} D_{44} a^6 h^4 \mu^4
\end{aligned}
$$

$$
\begin{aligned}
&h_{15} = -1156\pi^4 D_{12} D_{44} a^4 h^4 \lambda^2 \mu^2 \quad h_{16} = -578\pi^4 D_{12} D_{44} a^2 h^4 \lambda^4 \\
&h_{17} = 289\pi^4 D_{22} D_{44} a^6 h^4 \mu^2 \quad h_{18} = 289\pi^4 D_{22} D_{44} a^4 h^4 \lambda^2 \\
&h_{19} = 2856\pi^2 D_{22} D_{55} a^6 h^2 \lambda^2 \mu^2 \quad h_{20} = 2856\pi^2 D_{22} D_{55} a^4 h^2 \lambda^4 \\
&h_{21} = 2856\pi^2 D_{44} D_{55} a^6 h^2 \lambda^2 \mu^4 \quad h_{22} = 5712\pi^2 D_{44} D_{55} a^4 h^2 \lambda^4 \mu^2 \\
&h_{23} = 2856\pi^2 D_{44} D_{55} a^2 h^2 \lambda^6 \quad h_{24} = 2856\pi^2 D_{44} D_{66} a^6 h^2 \lambda^2 \mu^2 \\
&h_{25} = 2856\pi^2 D_{44} D_{66} a^4 h^2 \lambda^4 \quad h_{26} = 28224 D_{55} D_{66} a^6 \lambda^4 \mu^2 \\
&h_{27} = 28224 D_{55} D_{66} a^4 \lambda^6
\end{aligned} \tag{33}
$$

Paper 2

Local Buckling of Corrugated Board Facings

Ulf Nyman and Per Johan Gustafsson
Division of Structural Mechanics
Lund University

ECCM '99
European Conference on
Computational Mechanics
August 31 – September 3
München, Germany

LOCAL BUCKLING OF CORRUGATED BOARD FACINGS

Ulf Nyman and Per Johan Gustafsson
Division of Structural Mechanics
Lund University, Sweden
e–mail: ulf.nyman@byggmek.lth.se

Key words: Corrugated board, Local buckling, Transverse shear, Orthotropic, Rayleigh-Ritz, Periodic

Abstract. *Local buckling of corrugated board facings is studied numerically through finite element calculations. In addition, an analytical model is developed by the use of the Rayleigh-Ritz method. The facings are modeled as infinite orthotropic plates, resting on parallel free supports and subjected to an arbitrary in-plane stress state. The deflection shape is defined by wave length and displacement of the periodic deflection pattern. Transverse shear strain is considered by first (FEM) and higher order (analytical) shape functions. The results suggest that the low out-of-plane shear stiffness of paper significantly affect the critical load.*

1 Introduction

Corrugated paper board, Figure (1a), is extensively used within the packaging industry as a load bearing structure. Its wide application is due to an outstanding strength/cost value. In addition, the use of raw material from a renewable resource strengthens its position. In this work, local buckling of the facings of the board is studied for general in-plane loading, Figure (1b). The purpose is to find a criterion for local buckling that enables assessment of risk of buckling from state of stress without need for extensive numerical calculations. Such a criterion is needed for rational evaluation of the stresses in various parts of a package as determined by, e.g., linear finite element analysis. An approximate analytical criterion is proposed and compared to finite element analysis. The analytical and numerical analyses are valid for orthotropic plates in a general homogeneous in-plane state of stress and particular considerations are made to the transverse out-of-plane shear strains and to the periodic local buckling pattern of a facing of large size.

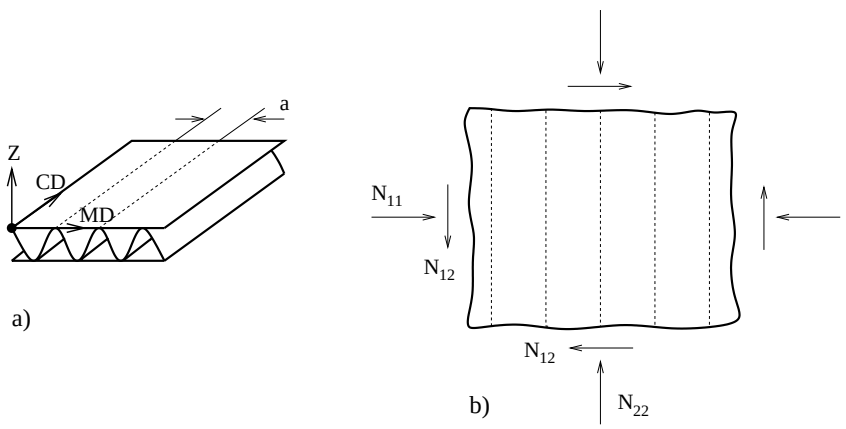

Figure 1: a) Corrugated paper board. b) Facing

The need for orthotropic material modeling and consideration to transverse shear deformation are due to the highly anisotropic stiffness properties of paper [10]. The ratio of the in-plane elastic modulus in the machine direction (MD) of paper to the elastic modulus in the cross-machine direction (CD) is typically in the order of 2, and as high ratio between elastic modulus in MD to transverse shear modulus as 600 is reported [10]. In the present analytical analysis the transverse shear is modeled by a higher order shear deformation theory according to Reddy [12] and Levinson (1980). In the numerical analysis, a finite element with constant shear strain according to the theory of Reissner is employed.

Research relating to buckling of corrugated paper board has recently been presented by Patel [1], including results from experiments on corrugated paper board cylinders subject to biaxial loading and also including references to previous studies of corrugated paper board. Previous theoretical buckling analyses that relate to the present study include work

by Johnsson and Urbanik [2], who analyzed a triangular core sandwich under uniaxial compression and concluded that buckling was initiated by local buckling of the facing. Analysis of an isotropic aluminum sheet sandwich carried out by Wittrick and Curzon [3] showed that buckling modes with inclined nodal lines, where the out-of-plane deflection is zero, are possible. A study of the buckling of an in-plane orthotropic truss core sandwich in axial compression has been presented by Zahn [5].

2 Boundary conditions and periodicity

The plate under consideration is assumed to be of infinite size, Figure (1b), with free parallel supports at distance a. The deflection pattern at buckling can be assumed to be periodic with wavelength 2λ in the direction along the supports and may be assumed to repeat it self from one inter-support strip to the next. Though the inter-support deflection fields are equal, they are in general displaced, i.e. in different phase.

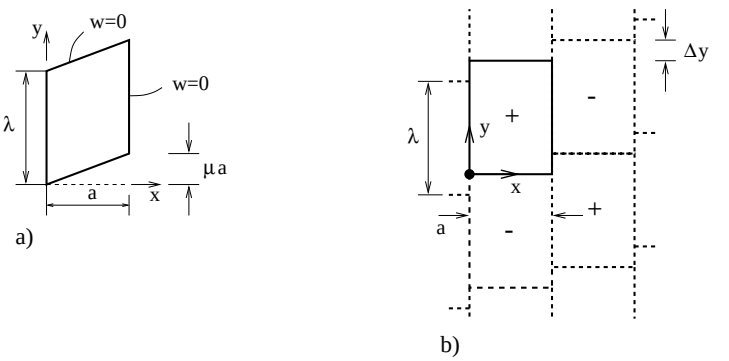

Figure 2: a) Periodic cell analyzed analytically. b) Periodic cell analyzed by FEM

In the analytical analysis approximate boundary conditions are adopted. A cell of length λ and width a is considered, Figure (2a). The deflection along the boundaries of this cell is assumed to be zero, i.e. $w = 0$ along the support lines $x = 0$ and $x = a$ and along inclined nodal lines $y = \mu x$ and $y = \lambda + \mu x$. The height of the cell, λ, and the inclination of the nodal lines, μ, are found by minimization of the critical load. Conditions regarding bending moment and shear strain along the boundaries of the cell can be obtained from the below, where shape functions for deflection and shear strain are defined.

In the finite element analysis a rectangular cell of height λ and width a is considered, see Figure (2b). Along $x = 0$ and $x = a$, w is zero. Other boundary conditions are defined by subsidiary conditions according to the periodic and anti-symmetric character of the deflection:

$$w(x,0) = -w(x,\lambda), \qquad \frac{\partial w}{\partial x}_{(x,0)} = -\frac{\partial w}{\partial x}_{(x,\lambda)}, \qquad \frac{\partial w}{\partial y}_{(x,0)} = -\frac{\partial w}{\partial y}_{(x,\lambda)} \tag{1}$$

and

$$\begin{aligned} \frac{\partial w}{\partial y}_{(0,y)} &= \frac{\partial w}{\partial y}_{(a,y-\lambda+\Delta y)}, & 0 < y < \lambda - \Delta y \\ \frac{\partial w}{\partial y}_{(0,y)} &= -\frac{\partial w}{\partial y}_{(a,y+\Delta y)}, & \lambda - \Delta y < y < \lambda \end{aligned} \tag{2}$$

Although all values > 0 of parameters λ and Δy yield buckling modes that are possible, only the pair of values that give the smallest critical load is of practical interest. The minimum of the critical load is determined numerically by FE calculations for various values of the parameters.

3 Analytical approach

The analytical approach in the present study is based upon the principle of stationary total potential strain energy. According to the higher order shear deformation theory due to Reddy [12], the plate displacement field is given by

$$\begin{aligned} u &= u^0 + z\psi_x - \frac{4z^3}{3h^2}\left(\frac{\partial w^0}{\partial x} + \psi_x\right) \\ v &= v^0 + z\psi_y - \frac{4z^3}{3h^2}\left(\frac{\partial w^0}{\partial y} + \psi_y\right) \\ w &= w^0 \end{aligned} \tag{3}$$

where u^0, v^0 and w^0 are mid-plane displacements and ψ_x, ψ_y are cross section rotations about the y-axis and x-axis respectively.

In order to introduce the displacement distribution over the plate region a Rayleigh-Ritz scheme is followed. Approximate displacement coordinate functions in consistency to the boundary conditions are used according to

$$\psi_i = q_i \phi_i \qquad i = 1, 2, 3 \tag{4}$$

in which $\psi_1 = w^{app}(x,y), \psi_2 = \psi_x^{app}(x,y), \psi_3 = \psi_y^{app}(x,y)$. The cross section rotation distributions are assumed to have the same form as the deflection derivative, i.e. $\phi_2 = w^0_{,x}, \phi_3 = w^0_{,y}$. This assumption was used by Harris and Auelmann [14] in analysis of plates considering first order shear deformation theory. Then the coordinate functions ϕ_i are given by

$$\begin{bmatrix} \phi_1 \\ \phi_2 \\ \phi_3 \end{bmatrix} = \begin{bmatrix} \mathrm{Im}\, e^{i\frac{\pi}{a}x} \mathrm{Im}\, e^{i[\frac{\pi}{\lambda}(y-p(x))]} \\ \frac{1}{a}\mathrm{Re}\, e^{i\frac{\pi}{a}x} \mathrm{Im}\, e^{i[\frac{\pi}{\lambda}(y-p(x))]} - \frac{\mu}{\lambda}\mathrm{Im}\, e^{i\frac{\pi}{a}x} \mathrm{Re}\, e^{i[\frac{\pi}{\lambda}(y-p(x))]} \\ \mathrm{Im}\, e^{i\frac{\pi}{a}x} \mathrm{Re}\, e^{i[\frac{\pi}{\lambda}(y-p(x))]} \end{bmatrix} \tag{5}$$

where $p(x)$ is a polynomial function of the nodal lines. In general, $p(x)$ is symmetric about a point centered in the x-direction. However, in this work the nodal lines are approximated as straight, i.e., $p(x) = \mu x$.

The elastic orthotropic constitutive behaviour is described by the stress-strain relation[1]

$$\boldsymbol{\sigma} = \begin{bmatrix} \sigma_{11} \\ \sigma_{22} \\ \sigma_{12} \\ \sigma_{13} \\ \sigma_{23} \end{bmatrix} = \boldsymbol{D\varepsilon} = \begin{bmatrix} D_{11} & D_{12} & D_{14} & D_{15} & D_{16} \\ & D_{22} & D_{24} & D_{25} & D_{26} \\ & & D_{44} & D_{45} & D_{46} \\ & sym. & & D_{55} & D_{56} \\ & & & & D_{66} \end{bmatrix} \begin{bmatrix} \varepsilon_{11} \\ \varepsilon_{22} \\ \gamma_{12} \\ \gamma_{13} \\ \gamma_{23} \end{bmatrix} \tag{6}$$

with

$$\begin{aligned} &D_{14} = D_{15} = D_{16} = D_{24} = D_{25} = D_{26} = D_{45} = D_{46} = D_{56} = 0 \\ &D_{11} = \frac{E_{xx}}{1 - \nu_{xy}\nu_{yx}},\ D_{12} = \frac{\nu_{yx}E_{xx}}{1 - \nu_{xy}\nu_{yx}},\ D_{22} = \frac{E_{yy}}{1 - \nu_{xy}\nu_{yx}} \\ &D_{44} = G_{xy},\ D_{55} = G_{xz},\ D_{66} = G_{yz} \end{aligned} \tag{7}$$

where E, G and ν are material constants. It is here undertaken that the material axes coincide with the coordinate axes of the plate. The kinematic relations are obtained by applying the small strain tensor format on (3)

$$\begin{aligned} \boldsymbol{\varepsilon} = \begin{bmatrix} \varepsilon_{11} \\ \varepsilon_{22} \\ \gamma_{12} \\ \gamma_{13} \\ \gamma_{23} \end{bmatrix} &= \begin{bmatrix} u^0_{,x} \\ v^0_{,y} \\ v^0_{,x} + u^0_{,y} \\ w^0_{,x} + \psi_x \\ w^0_{,y} + \psi_y \end{bmatrix} + z \begin{bmatrix} \psi_{x,x} \\ \psi_{y,y} \\ \psi_{y,x} + \psi_{x,y} \\ 0 \\ 0 \end{bmatrix} \\ &- \tfrac{4z^2}{h^2} \begin{bmatrix} 0 \\ 0 \\ 0 \\ w^0_{,x} + \psi_x \\ w^0_{,y} + \psi_y \end{bmatrix} - \tfrac{4z^3}{3h^3} \begin{bmatrix} w^0_{,xx} + \psi_{x,x} \\ w^0_{,yy} + \psi_{y,y} \\ \psi_{y,x} + \psi_{x,y} + 2w^0_{xy} \\ 0 \\ 0 \end{bmatrix} \end{aligned} \tag{8}$$

in which h denotes the thickness of the plate.

By defining the initial in-plane loading matrix $\mathbf{N}$ for the plate

$$\mathbf{N} = \begin{bmatrix} N_{11} \\ N_{12} \\ N_{22} \end{bmatrix} \tag{9}$$

the elastic strain energy varying during buckling can be obtained [7] by integrating over the plate region

$$U_1 = \frac{1}{2} \int \int_A N_{ij} w_{,i} w_{,j} dA \qquad i,j = 1,2 \tag{10}$$

$$U_2 = -\frac{1}{2} \int \int \int_V \sigma_{ij} \varepsilon_{ij} dV = -\frac{1}{2} \int \int \int_V \left[D_{11}\varepsilon_{11}^2 + 2D_{12}\varepsilon_{11}\varepsilon_{22} + D_{22}\varepsilon_{22}^2 + D_{44}\gamma_{12}^2 \right] dV \qquad i,j = 1,2 \tag{11}$$

$$U_3 = -\frac{1}{2} \int \int \int_V G_{ij}\gamma_{ij}\gamma_{ij} dV \qquad i = 1,2;\ j = 3 \tag{12}$$

[1]The stiffness coefficients where originally denoted A_{ij}

where U_2 is addressed to the in plane stress whereas U_3 is due to the out-of-plane shear stress. If (4) is substituted in (8) and integration of (11) and (12) is performed over the plate thickness from $z = -h/2$ to $z = h/2$, the following is obtained

$$U_2 = -\frac{1}{2}\int\int_A \frac{D_{ij}h^3}{315}\left(\frac{5}{4}w_{,ii}w_{,jj} - 4w_{,ii}\psi_{j,j} - 4w_{,jj}\psi_{i,i} + 17\psi_{i,i}\psi_{j,j}\right) + \frac{D_{kk}h^3}{315}(1-\delta_{ij})\left(\frac{5}{2}w_{,ij}w_{,ji} - 16w_{,ij}\psi_{i,j} + 17\psi_{i,j}\psi_{j,i} + 17\psi_{i,j}\psi_{i,j}\right)dA \qquad i,j = 1,2;\ k = 4 \tag{13}$$

$$U_3 = -\frac{1}{2}\int\int_A \frac{8h}{15}G_{ij}\left(w_{,i} + \psi_i\right)^2 dA \qquad i = 1,2;\ j = 3 \tag{14}$$

where δ_{ij} is the Kronecker delta function. The equilibrium condition of the plate can be expressed by a stationary first variation of energy. According to (10), (11) and (12) this is expressed as

$$\delta\Pi = 0 \quad \rightarrow \quad \frac{\partial\Pi}{\partial q_i} = 0 \quad i = 1,2,3 \tag{15}$$

Π being defined as the energy functional[2] $\Pi = U_1 + U_2 + U_3$.

In order to find the complete solution of the critical state the energy functional in (15) should be minimized with respect to both q_i and λ, μ. The approximative displacement coordinate functions given by (4) will produce a set of equations in w^{app}, ψ_x^{app} and ψ_y^{app} which are not linear. However, a non-linear equation system in q_i and λ, μ is not desired since a numerical procedure required to find the critical solution would involve producing initial guess values. This is straight forward for λ and μ, whereas q_i are of more arbitrary form making it difficult to find an automated solution process. Therefore the solution strategy chosen is first solving for q_i in a linear sense, and then use this solution to find the parameters λ and μ.

The expression for Π can be determined by evaluating (10), (13) and (14) for the given set of displacement functions. By then applying (15) on Π the following homogeneous equation system is obtained

$$B_{ij}\psi_j = 0 \qquad i,j = 1,2,3 \tag{16}$$

where the coefficients B_{ij} are given in appendix.

The critical state of (16) is given by the singularity condition on B_{ij}, i.e. $\det(B_{ij}) = 0$. Applying this and using the parameterization

$$\mathbf{N} = \hat{N}\begin{bmatrix}\alpha\\ \beta\\ \chi\end{bmatrix} \tag{17}$$

[2]Original sign convention; $\Pi = U_1 - U_2 - U_3$

the critical stress state is expressed by the load function

$$\hat{N}(\lambda,\mu) = \frac{G}{60a^2\lambda^2\left(c_2\alpha + 2a^2\beta\mu + a^2\chi\right)H} \tag{18}$$

where

$$G = \sum_{i=1}^{33} g_i \qquad H = \sum_{i=1}^{27} h_i \tag{19}$$

The coefficients g_i, h_i and c_2 are given in Appendix.

The minimum of $\hat{N}$, $\hat{N}_{cr}$, is now only determined by the parameters $\bar{x} = (\lambda/a, \mu)$. In order to find the values of $\bar{x}$ that minimizes (18) a simplex search [8] is used.

4 Finite element setup

The finite element calculations are performed for the purpose of studying the character of the periodicity and finding the conditions under which the true critical load is present for the complete structure.

The two parameters to be studied are λ and Δy in Figure (2b). The variation of λ is performed by adding one element for each step considered. The application of the periodic boundary conditions as well as the reference edge loads is automatically created for every mesh. The variation of Δy is carried out by initially couple two horizontal nodes equally in magnitude but opposite sign, i.e. $\Delta y = 0$, for every mesh. Then a phase difference is incorporated by gradually increase the y-distance for which two nodes are coupled.

For the convenience, by means of programming, a four node linear interpolation element is chosen. The element incorporates constant shear deformation through the thickness. This makes the comparison with the analytical solution somewhat awkward but the only available since higher order shear elements are not implemented. The element has six degrees of freedom per node and uses reduced stiffness integration, see Hibbitt et al. [9]. Different mesh densities was tried for a uniaxially loaded simply supported quadratic plate and it was concluded that a 20×20 mesh only differed from the exact solution [13] by 1%, in terms of the critical load. Considering the large number of problems to solve, no finer resolution of the mesh was chosen for the parameter study.

The stiffness and geometrical properties, chosen as an example of representative properties for corrugated board facings, are listed in Table (4).

5 Results

In the following results are presented for the material parameters in Table (4). The reference load in the y-direction is held constant at $\chi = 1$ and the in-plane shear load is

Parameter	*Value*
E_{xx}	7 [GPa]
E_{yy}	$E_{xx}/2$
G_{xy}	$E_{xx}/3$
G_{xz}	$E_{xx}/300$
G_{yz}	$E_{xx}/30$
ν_{xy}	0.2
a	7 [mm]
h	$a/20$ [mm]

Table 1: Stiffness and geometrical properties.

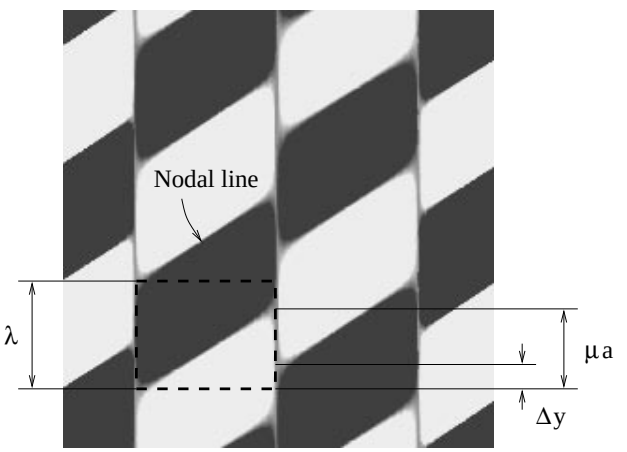

Figure 3: Out-of-plane deformation plot.

increased at steps in the interval $0 < \beta < 10$. For the purpose of comparison a non-dimensionalized buckling coefficient is computed according to

$$K_{cr} = \frac{a^2 \hat{N}_{cr}}{\pi^2 D_{11}} (\alpha + \beta + \chi) \tag{20}$$

In the FEM calculations λ/a is defined as the ratio of the number of elements in the y-direction to the number of elements in the x-direction. In a similar manner $\Delta y/a$ is defined as the ratio of the number of elements the phase shift is applied in the current solution to the number of elements in the x-direction. μ is measured in an approximate manner from the deformation plots, as the slope of the line between two points where $w = 0$, located at $x = 0.2\,a$ and $x = 0.8\,a$, respectively. An example of an array of unified cells is showed in Figure (3), where the absolute deformations larger than 1% of the maximum deformation is filtered for clarity.

For every set of reference loads the FEM parameter solution that yields the least buckling

coefficient $\min(K) = K_{cr}$ is sought, together with the corresponding parameters $\Delta y/a$ and λ/a. An example of the buckling coefficient K calculated by FEM is given in Figure (4) for the case $\alpha = 0, \beta = 5$ and $\chi = 1$.

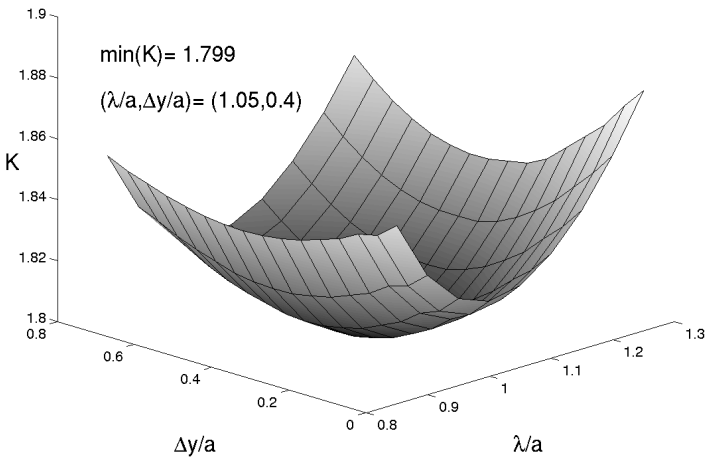

Figure 4: Buckling coefficient calculated by FEM.

From Table (5) it is seen that when the normal load and shear load are of the same the same order of magnitude, the buckling coefficients from the different models are in good agreement. The discrepancy between the FEM solution and the approximate analytical solution is largest at $\beta = 10$, 5%. It should be noted that the case $\beta = 0, \chi = 1$, i.e. the two left columns in the upper row in (5), yields the exact solution, since no enforcement of the boundary conditions is inferred by assuming straight nodal lines.

It is marked that the phase shift $\Delta y/a$ differs from the value of μ for this material. However from Figure (4) it follows that the buckling coefficient is more sensitive for variations in λ than for variations in Δy. This is even more pronounced from the FEM calculations at low values of the shear load, which suggests that the plate can be approximated as finite in the x-direction, i.e. not considering the cyclic boundary conditions at the supports, during buckling analysis.

The values of K_{cr} with increasing shear load from Table (5) are also plotted[3] in Figure (5). As a comparison to the value of the buckling coefficient when neglecting the transverse shear, a material with large transverse shear modulus is studied, see the upper solid line in Figure (5). It is seen that the difference between considering and not considering the

[3]HSDPT – Higher order shear deformation plate theory.
FSDPT – First order shear deformation plate theory.

β	$\Delta y/a$	$\bar{x}^a$	K^a_{cr}	$\bar{x}^b$	K^b_{cr}
0	0	(0.85,0)	1.742	(0.867,0)	1.751
0.2	0	(0.9,0.2)	2.011	(0.868,0.179)	2.03
0.4	0.1	(0.9,0.35)	2.125	(0.873,0.341)	2.165
0.6	0.2	(0.9,0.5)	2.147	(0.882,0.469)	2.204
0.8	0.25	(0.95,0.6)	2.131	(0.893,0.564)	2.199
1	0.3	(0.95,0.7)	2.101	(0.903,0.634)	2.177
1.5	0.3	(1,0.8)	2.025	(0.922,0.749)	2.11
3	0.35	(1,0.9)	1.881	(0.949,0.89)	1.973
5	0.4	(1.05,0.95)	1.799	(0.963,0.954)	1.892
10	0.45	(1.05,1.1)	1.726	(0.974,1.005)	1.818

[a]FEM
[b]Analytical model

Table 2: Nondimensionalized buckling coefficients.

transverse shear is large for all of the analyzed load combinations. For the chosen material parameters the buckling coefficient is relatively constant with increasing in-plane shear load. When no transverse shear is present, i.e. pure bending, the buckling load is increased by 56% for the same load case.

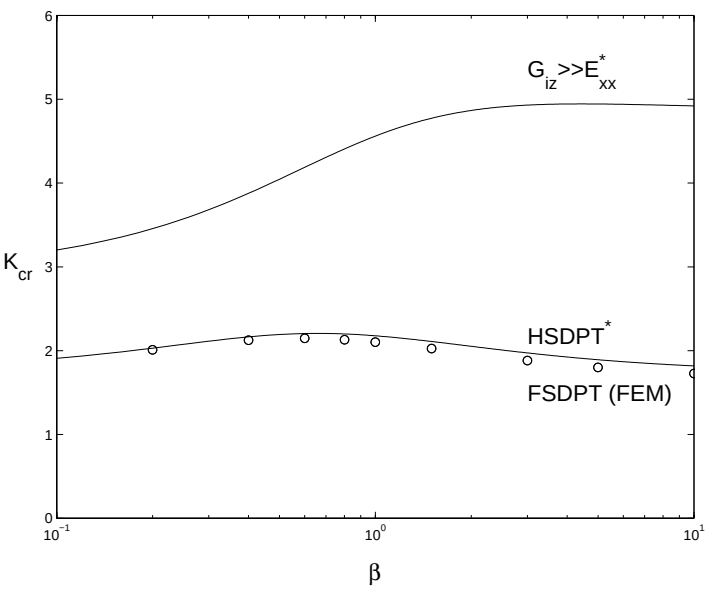

Figure 5: Buckling coefficient with increasing shear load. *Present model.

6 Conclusions

A method of finding the critical load for a transverse shear flexible plate subject to arbitrary in-plane load is developed. The plate is in the analytical model treated as long, simply supported along the long end lines. In the FEM calculations a cell periodically repeating itself is studied. Cyclic boundary conditions are applied along all edges of the cell. The proposed method is in good agreement with the results gained from the finite element analysis. The method also proves to be computationally efficient.

For the chosen material properties, representative that of paper, the buckling coefficient is significantly reduced by the transverse shear deformations, even though the plate width to thickness ratio is 20. For the uniaxial load case, the buckling coefficient is lowered by 39%, whereas under in plane shear load, the same reduction is 64%. It is observed that in contrast to the case when no shear deformations are considered, the buckling coefficient is relatively constant with increasing in plane shear load. When no transverse shear is present, i.e. pure bending, the buckling load is increased by 56% for the same load case.

References

[1] P. Patel. *Biaxial Failure of Corrugated Board.* KFS AB, (1996)

[2] M. W. Johnson and T. J. Urbanik. *Analysis of the Localized Buckling in Composite Plate Structures with application to Determining the Strength of Corrugated Fiberboard.* J. of Composites Technology and Research, Vol. 11, No. 4, pp. 121-127, (1989)

[3] W. H. Wittrick and P. L. V. Curzon. *Buckling of a Series of Equidistant Longitudinal Supports in Combined Longitudinal Compression and Shear.* The Aeronautical Quarterly, (1969)

[4] W. H. Wittrick and P. L. V. Curzon. *Nodal Lines for Long Plates in Combined Shear and Compression with Sinusoidal Edge Rotations.* The Aeronautical Quarterly, Vol. XX, (1969)

[5] J. J. Zahn. *Local Buckling of Orthotropic Truss-Core Sandwich.* Research paper, USDA Forest Service, (1973)

[6] M. S. Anderson. *Local Instability of the Elements of a Truss-Core Sandwich Plate.* NACA Tech, Note 4292, July (1958)

[7] Z. P. Bazant *Stability of Structures.* Oxford University Press, (1991)

[8] J. A. Nelder and R. Mead. *A Simplex Method for Function Minimization*, Computer Journal, vol. 7, pp 308-313

[9] Hibbitt, Karlsson, Sorensen Inc., *ABAQUS/Standard Version 5.8*, Pawtucket, RI, (1998)

[10] K. Persson, *Material Model for Paper: Experimental and Theoretical Aspects*, Diploma Report, Lund University, Sweden, (1991)

[11] E. Reissner, *The Effect of Transverse Shear Deformation on the Bending of Elastic Plates*, J. Appl. Mech., 12, A69-A77, (1945)

[12] J. N. Reddy, *A Simple Higher-Order Theory for Laminated Composite Plates*, J. Appl. Mech., 51(4), 745-752, Dec. (1984)

[13] J. N. Reddy and N. D. Phan, *Stability and Vibration of Isotropic, Orthotropic and Laminated Plates According to a Higher-Order Shear Deformation Theory*, J. of Sound and Vibration, **98**(2), 157-170, (1985)

[14] L. A. Harris and R. A. Auelmann, *Stability of flat simply-supported, corrugated-core sandwich plates under combined loads.*, J. Aero/Space Sci., **27**, 7, pp 525-534 July (1960)

[15] P. Seide, *Comments on "Stability of flat simply-supported, corrugated-core sandwich plates under combined loads".*, J. Aerospace Sci., **28**, 3, p 248 March (1961)

Appendix

The coefficients B_{ij}:

$$
\begin{aligned}
B_{11} &= -\frac{c_1}{5040a^3h^2\lambda^3}\left[-5D_{11}c_1c_3h - 10a^2c_1c_2h(D_{12}+2D_{44}) - 5D_{22}a^4c_1h\right. \\
&\quad \left. -672a^2h\lambda^2(D_{55}c_2+D_{66}a^2) + 1260a^2\lambda^2(N_{11}c_2+2N_{12}a^2\mu+N_{22}a^2)\right] \\
B_{12} &= \frac{\pi h}{315a^3\lambda^3}\left[-D_{11}c_1c_3 - a^2c_1c_2(D_{12}+2D_{44}) + 42D_{55}a^2c_2\lambda^2\right] \\
B_{13} &= -\frac{\pi h}{315a\lambda^2}\left[c_1c_2(D_{12}+2D_{44}) + D_{22}a^2c_1 - 42D_{66}a^2\lambda^2\right] \\
B_{22} &= \frac{h}{1260a^3\lambda^3}\left[17D_{11}c_1c_3 + 17D_{44}a^2c_1c_2 + 168D_{55}a^2c_2\lambda^2\right] \\
B_{23} &= \frac{17c_1c_2h}{1260a\lambda^2}(D_{12}+D_{44}) \\
B_{33} &= \frac{h}{1260a\lambda^3}\left[17D_{44}c_1(4a^4\mu^4 - 5a^2c_2\mu^2 - c_3)\right. \\
&\quad \left. +17D_{22}a^2c_1(c_2 - a^2\mu^2) + 168D_{66}a^2\lambda^4)\right] \\
B_{21} &= B_{12},\ B_{31} = B_{13},\ B_{32} = B_{23} \\
c_1 &= \pi^2h^2,\ c_2 = \lambda^2 + a^2\mu^2,\ c_3 = \lambda^4 + 6a^2\lambda^2\mu^2 + a^4\mu^4
\end{aligned}
\tag{21}
$$

The fraction coefficients g_i and h_i:

$$
\begin{aligned}
&g_1 = 17\pi^6 c_3^2 D_{11}^2 D_{22} a^2 h^7 \quad g_2 = 17\pi^6 c_2 c_3^2 D_{11}^2 D_{44} h^7 \\
&g_3 = 168\pi^4 c_3^2 D_{11}^2 D_{66} a^2 h^5 \lambda^2 \quad g_4 = -17\pi^6 c_3 c_2^2 D_{11} D_{12}^2 a^2 h^7 \\
&g_5 = 34\pi^6 c_2 c_3 D_{11} D_{12} D_{22} a^4 h^7 \quad g_6 = 336\pi^4 c_2 c_3 D_{11} D_{12} D_{66} a^4 h^5 \lambda^2 \\
&g_7 = 17\pi^6 c_3 D_{11} D_{22}^2 a^6 h^7 \quad g_8 = 102\pi^6 c_2 c_3 D_{11} D_{22} D_{44} a^4 h^7 \\
&g_9 = 14280\pi^4 c_2 c_3 D_{11} D_{22} D_{55} a^4 h^5 \lambda^2 \quad g_{10} = 14280\pi^4 c_3 D_{11} D_{22} D_{66} a^6 h^5 \lambda^2 \\
&g_{11} = 68\pi^6 c_3 c_2^2 D_{11} D_{44}^2 a^2 h^7 \quad g_{12} = 14280\pi^4 c_3 c_2^2 D_{11} D_{44} D_{55} a^2 h^5 \lambda^2 \\
&g_{13} = 14952\pi^4 c_2 c_3 D_{11} D_{44} D_{66} a^4 h^5 \lambda^2 \\
&g_{14} = 141120\pi^2 c_2 c_3 D_{11} D_{55} D_{66} a^4 h^3 \lambda^4 \\
&g_{15} = -34\pi^6 c_2^3 D_{12}^3 a^4 h^7 \quad g_{16} = -17\pi^6 c_2^2 D_{12}^2 D_{22} a^6 h^7 \\
&g_{17} = -136\pi^6 c_2^3 D_{12}^2 D_{44} a^4 h^7 \quad g_{18} = -14112\pi^4 c_2^3 D_{12}^2 D_{55} a^4 h^5 \lambda^2 \\
&g_{19} = -14112\pi^4 c_2^2 D_{12}^2 D_{66} a^6 h^5 \lambda^2 \quad g_{20} = 336\pi^4 c_2^2 D_{12} D_{22} D_{55} a^6 h^5 \lambda^2 \\
&g_{21} = -136\pi^6 c_2^3 D_{12} D_{44}^2 a^4 h^7 \quad g_{22} = -27888\pi^4 c_2^3 D_{12} D_{44} D_{55} a^4 h^5 \lambda^2 \\
&g_{23} = -27888\pi^4 c_2^2 D_{12} D_{44} D_{66} a^6 h^5 \lambda^2 \quad g_{24} = 282240\pi^2 c_2^2 D_{12} D_{55} D_{66} a^6 h^3 \lambda^4 \\
&g_{25} = 17\pi^6 c_2 D_{22}^2 D_{44} a^8 h^7 \quad g_{26} = 168\pi^4 c_2 D_{22}^2 D_{55} a^8 h^5 \lambda^2 \\
&g_{27} = 68\pi^6 c_2^2 D_{22} D_{44}^2 a^6 h^7 \quad g_{28} = 14952\pi^4 c_2^2 D_{22} D_{44} D_{55} a^6 h^5 \lambda^2 \\
&g_{29} = 14280\pi^4 c_2 D_{22} D_{44} D_{66} a^8 h^5 \lambda^2 \quad g_{30} = 141120\pi^2 c_2 D_{22} D_{55} D_{66} a^8 h^3 \lambda^4 \\
&g_{31} = 672\pi^4 c_2^3 D_{44}^2 D_{55} a^4 h^5 \lambda^2 \quad g_{32} = 672\pi^4 c_2^2 D_{44}^2 D_{66} a^6 h^5 \lambda^2 \\
&g_{33} = 564480\pi^2 c_2^2 D_{44} D_{55} D_{66} a^6 h^3 \lambda^4
\end{aligned} \tag{22}
$$

$$
\begin{aligned}
&h_1 = 289\pi^4 D_{11} D_{22} a^6 h^4 \mu^4 \quad h_2 = 1734\pi^4 D_{11} D_{22} a^4 h^4 \lambda^2 \mu^2 \\
&h_3 = 289\pi^4 D_{11} D_{22} a^2 h^4 \lambda^4 \quad h_4 = 289\pi^4 D_{11} D_{44} a^6 h^4 \mu^6 \\
&h_5 = 2023\pi^4 D_{11} D_{44} a^4 h^4 \lambda^2 \mu^4 \quad h_6 = 2023\pi^4 D_{11} D_{44} a^2 h^4 \lambda^4 \mu^2 \\
&h_7 = 289\pi^4 D_{11} D_{44} h^4 \lambda^6 \quad h_8 = 2856\pi^2 D_{11} D_{66} a^6 h^2 \lambda^2 \mu^4 \\
&h_9 = 17136\pi^2 D_{11} D_{66} a^4 h^2 \lambda^4 \mu^2 \quad h_{10} = 2856\pi^2 D_{11} D_{66} a^2 h^2 \lambda^6 \\
&h_{11} = -289\pi^4 D_{12}^2 a^6 h^4 \mu^4 \quad h_{12} = -578\pi^4 D_{12}^2 a^4 h^4 \lambda^2 \mu^2 \\
&h_{13} = -289\pi^4 D_{12}^2 a^2 h^4 \lambda^4 \quad h_{14} = -578\pi^4 D_{12} D_{44} a^6 h^4 \mu^4 \\
&h_{15} = -1156\pi^4 D_{12} D_{44} a^4 h^4 \lambda^2 \mu^2 \quad h_{16} = -578\pi^4 D_{12} D_{44} a^2 h^4 \lambda^4 \\
&h_{17} = 289\pi^4 D_{22} D_{44} a^6 h^4 \mu^2 \quad h_{18} = 289\pi^4 D_{22} D_{44} a^4 h^4 \lambda^2 \\
&h_{19} = 2856\pi^2 D_{22} D_{55} a^6 h^2 \lambda^2 \mu^2 \quad h_{20} = 2856\pi^2 D_{22} D_{55} a^4 h^2 \lambda^4 \\
&h_{21} = 2856\pi^2 D_{44} D_{55} a^6 h^2 \lambda^2 \mu^4 \quad h_{22} = 5712\pi^2 D_{44} D_{55} a^4 h^2 \lambda^4 \mu^2 \\
&h_{23} = 2856\pi^2 D_{44} D_{55} a^2 h^2 \lambda^6 \quad h_{24} = 2856\pi^2 D_{44} D_{66} a^6 h^2 \lambda^2 \mu^2 \\
&h_{25} = 2856\pi^2 D_{44} D_{66} a^4 h^2 \lambda^4 \quad h_{26} = 28224 D_{55} D_{66} a^6 \lambda^4 \mu^2 \\
&h_{27} = 28224 D_{55} D_{66} a^4 \lambda^6
\end{aligned} \tag{23}
$$

Paper 3

Material and Structural Failure Criterion of Corrugated Board Facings

Ulf Nyman and Per Johan Gustafsson
Division of Structural Mechanics
Lund University

Material and Structural Failure Criterion of Corrugated Board Facings

By Ulf Nyman[1] and Per Johan Gustafsson[2]

ABSTRACT: A failure stress criterion for corrugated board facings is presented. The failure criterion is based on material failure and structural local buckling failure, which are evaluated in a combined analysis procedure. The failure stress is compared with collapse experiments on corrugated board cylinders and the failure stress presented herein is seen to be in much better agreement with the measured stresses than the Tsai-Wu failure criterion alone. The fluting wavelength of the corrugated board is also varied for the purpose of strength sensitivity analysis of corrugated board.

Introduction

The strength of corrugated board is of great importance whithin the industry. Accurate design methods are crucial in determining the load capacity of corrugated board. Strength analysis of corrugated board has previously been devoted to calculations on material failure criterions, such as the Tsai-Wu [8] tensor polynomial criterion and modifications of this [7].

Reduction of strength in the compressive region due to local instability of the facing has been found in several investigations [6, 3, 9], and recently, a buckling criterion for the facing was developed for evaluation of the bifurcation load given a general in-plane stress state [5]. For potential material failure points it is hence possible to determine the likeliness of local buckling. An example of buckling induced strength reduction in the compressive region is shown in Figure 1.

The development of the finite element method have led to largely extended opportunities by means of calculations on structural response. However, the detailed modeling of corrugated board is both demanding in terms of pre-processing as well as numerical intensive in the solution process. Therefore, a failure criterion for stress evaluation based on simplified finite element calculations, e.g. composite shell analysis, is vindicated. Herein, a comparison between material failure and structural failure is presented along with a method of determining wich failure mode is decisive. Numerical results of a representative board are illustrated in figures for various biaxial stresses and shear stresses.

[1]Structural Mechanics, Lund University, PO Box 118, S-221 00 Lund, Sweden.
[2]Structural Mechanics, Lund University, Sweden.

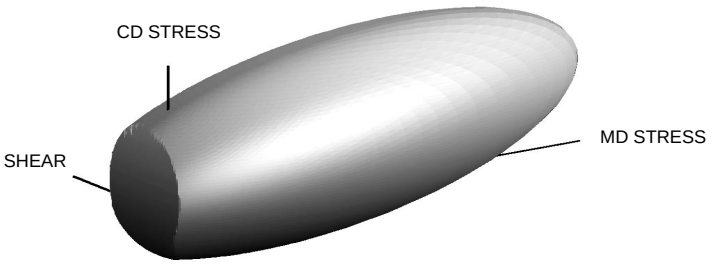

Figure 1: Reduction of strength in compressive region.

Choice of coordinate system

The in-plane stresses in the facings are referred to as normal stresses in the machine direction (MD) and cross direction (CD), and shear. However, for convenience, in further calculations the stresses σ_{11}, σ_{22} and σ_{12} will be used, ordered as previously, given in the coordinates x_1, x_2 and x_4.

Generally, material failure defines a limit surface about the origin in stress space $\{\sigma_{11}, \sigma_{12}, \sigma_{22}\}$. Therefore, in analyzing the in-plane stresses, it may be suitable to express the stresses in spherical coordinates. Then, the cartesian stresses transform according to

$$\begin{aligned} \sigma_{11} &= \sigma^R \sin\phi \cos\theta \\ \sigma_{12} &= \sigma^R \sin\phi \sin\theta \qquad\qquad 0 \le \phi \le \pi,\ 0 \le \theta \le 2\pi \\ \sigma_{22} &= \sigma^R \cos\phi \end{aligned} \tag{1}$$

where σ^R is the length of a stress vector $\boldsymbol{\sigma}$, from the the origin O to the stress point S in stress space, i.e. $\sigma^R = \|\boldsymbol{\sigma}\|$. Moreover, ϕ is the angle $\boldsymbol{\sigma}$ makes with the positive direction of the x_2-axis, and θ is the angle between the plane containing S and the x_2-axis and the plane containing the x_1-axis and the x_2-axis, see Figure 2.

Material failure

A commonly used material failure criterion for paper is the Tsai-Wu orthotropic tensor polynomial [8]. In using the Tsai-Wu criterion, tensile and compressive strength parameters must be measured for both MD and CD. In addition, the shear strength and the equibiaxial tensile strength must be determined. The latter is determined by equally increasing the MD-stress and CD-stress to the limit state. However, approximations for the shear strength and equibiaxial strength have proven to be reasonable for paper [1].

The Tsai-Wu criterion for plane stress is given by

$$\Phi_{tw} = F_1\sigma_{11} + F_2\sigma_{22} + F_{11}\sigma_{11}^2 + F_{22}\sigma_{22}^2 + F_{66}\sigma_{12}^2 + 2F_{12}\sigma_{11}\sigma_{22} \le 1 \tag{2}$$

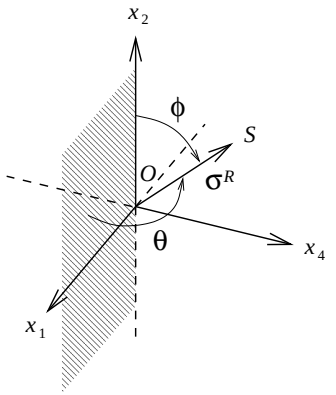

Figure 2: Coordinate system.

where

$$F_1 = \frac{1}{X_t} + \frac{1}{X_c}, \quad F_2 = \frac{1}{Y_t} + \frac{1}{Y_c}, \quad F_{11} = -\frac{1}{X_t X_c}, \quad F_{22} = -\frac{1}{Y_t Y_c}, \quad F_{66} = \frac{1}{T^2} \tag{3}$$

with the notation

$$\begin{aligned} X_t &= \text{Tensile strength in MD} \\ X_c &= \text{Compressive strength in MD} \\ Y_t &= \text{Tensile strength in CD} \\ Y_c &= \text{Compressive strength in CD} \\ T &= \text{Shear strength} \end{aligned} \tag{4}$$

An approximation for F_{12} is given by $F_{12} = f\sqrt{F_{11}F_{22}}$, where the constant $f = -0.36$ can be used for paper, see [1]. Moreover, the shear strength can be calculated as $T = \alpha\sqrt{X_c Y_c}$, where the parameter α can be derived using a maximum strain theory, where the compressive strengths X_c and Y_c are transformed to an equivalent shear stress, see [2]. The usefulness of the formulas for F_{12} and T is certainly justified by the difficulties emerging in corresponding experimental procedures.

Structural failure

The local buckling criterion given in [5] can be used to determine the stress state at which the facing becomes instable. The buckling equation is given by

$$\hat{N}_{cr} = \frac{\sum_{i=1}^{33} g_i}{60a^2\lambda^2\left(c_2\alpha + 2a^2\beta\mu + a^2\chi\right)\sum_{i=1}^{27} h_i} \qquad [\lambda, \mu] \in \mathbf{x}_{cr} \tag{5}$$

where α, β and χ relates to the MD-load, shear load and CD-load, respectively. Moreover, λ is the half buckling wavelength and μ is the inclination of nodal lines, indicating the

slope of the buckling deformation pattern. The parameter a denotes the wavelength of the corrugated core, where the corrugations are oriented in the facing machine direction. See [5] for the coefficients g_i and h_i.

In (5), $\mathbf{x}_{cr}$ is the solution of λ and μ at the buckling load, i.e. the bifurcation point. The solution $\mathbf{x}_{cr}$ is found by numerical minimization of the buckling load equation, which can be performed at points where buckling is suspected.

The buckling solution given in (5) relates to the edge load, i.e. force per unit length. The relation between the critical stress and the critical edge load is found from

$$\boldsymbol{\sigma}_{cr} = \begin{bmatrix} \sigma_{11} \\ \sigma_{12} \\ \sigma_{22} \end{bmatrix}_{cr} = \frac{1}{h}\mathbf{N}_{cr} = \frac{\hat{N}_{cr}}{h} \begin{bmatrix} \alpha \\ \beta \\ \chi \end{bmatrix} \tag{6}$$

in which h is the facing thickness.

Combined failure criterion

In order to determine which failure mode is most significant, material failure and structural failure must be compared. This seems to be of relevance when either some of the normal stresses is dominantly compressive or the shear stress is large. Below, the material failure criterion is reformulated followed by a similar modification of the structural failure criterion, i.e. the buckling equation.

Firstly, by using the transformation in (1), the Tsai-Wu criterion (2) takes the form

$$\begin{aligned} &(F_{11}\sin^2\phi\cos^2\theta + F_{22}\cos^2\phi + F_{66}\sin^2\phi\sin^2\theta + 2F_{12}\sin\phi\cos\phi\cos\theta)(\sigma_{tw}^R)^2 + \\ &(F_1\sin\phi\cos\theta + F_2\cos\phi)\sigma_{tw}^R - 1 = 0, \qquad\qquad \sigma_{tw}^R > 0 \end{aligned} \tag{7}$$

and the radius σ_{tw}^R can be found explicitly at a given stress state from (7), where ϕ and θ is given by the inverse of (1).

Next, in a similar manner, the buckling equation (5) can be rewritten using (1). As the load defined in (5) takes positive sign for compressive load, the normal in-plane loads change sign using the same convention as in (7). Moreover, the absolute value for shear load is used, due to symmetry. Then, (5) takes the form

$$\sigma_{cr}^R = \frac{\sum_{i=1}^{33} g_i}{60a^2h\lambda^2\left(-c_2 n_{11} + 2a^2\mu|n_{12}| - a^2 n_{22}\right)\sum_{i=1}^{27} h_i} \qquad \sigma_{cr}^R > 0,\ [\lambda,\mu] \in \mathbf{x}_{cr} \tag{8}$$

where

$$n_{11} = \sin\phi\cos\theta \qquad n_{12} = \sin\phi\sin\theta \qquad n_{22} = \cos\phi \tag{9}$$

To find the buckling load parameter σ_{cr}^R, 8 is minimized numerically with respect to λ and μ. This minimization is sensitive to the principles in how the initial values of $\mathbf{x}_{cr}$, $\mathbf{x}_0$, are chosen. By inspection of (8), it can be concluded that $\sigma^R(\lambda,\mu)$ is discontinous at $\lim_{\sigma^R\to\infty}\mathbf{x}$. This is certainly expressed when the load changes from a dominant compressive σ_{11}-stress, yielding a very large buckling wavelength and zero inclination of nodal lines, to a shear buckling mode with $\lambda \approx a$ and non-zero μ. The relation between λ and

μ, at a given relation of stresses, by which $\sigma^R \to \infty$, can be obtained from (8). In order to find the true solution of σ^R, σ^R_{cr}, the initial values $\mathbf{x}_0$ must be chosen on both sides of the values $\lim_{\sigma^R \to \infty} \mathbf{x}$.

When analyzing the stresses in the facing, e.g. corrugated board design, the least of σ^R_{cr} and σ^R_{tw} should be chosen. This is done by defining the distance from the origin to the stress point at failure, either material failure or structural failure, as the failure stress radius σ^R_f

$$\sigma^R_f = \min\left\{\sigma^R_{tw}, \sigma^R_{cr}\right\} \tag{10}$$

In Figure 3 the failure stress radius is shown as the least envelope of material failure and structural failure. From a given state of stress $\boldsymbol{\sigma}$, provided by e.g. finite element analysis,

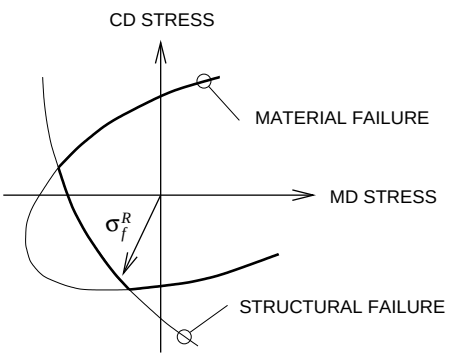

Figure 3: Failure stress radius.

a failure index Φ can be calculated

$$\Phi(\sigma_{11}, \sigma_{12}, \sigma_{22}) = \frac{||\boldsymbol{\sigma}||}{\sigma^R_f} \tag{11}$$

This failure index increases as the actual stress increases and takes the unity value at failure. It should be observed that the failure index, Φ, is not fundamentally the same as the Tsai-Wu index, Φ_{tw}, i.e. the left side of equation (2). Φ, but not Φ_{tw}, is proportional to the stress radius σ^R, defined in the second chapter.

The procedure for stress evaluation in a design process can be explained in the following chronological sequence

1. From finite element analysis, e.g. composite shell calculations, determine the stresses at various points of the corrugated panel. Perform the following steps for all of the points at which failure analysis is of interest.

2. Calculate by equation (1) the parameters ϕ and θ from the given MD stress, CD stress and shear stress.

3. Determine σ^R_{tw} by solving equation (7).

4. Determine the critical point, $\mathbf{x}_{cr}$ and σ_{cr}^R, by minimization of (5). For this minimization, a non-linear unconstrained procedure should be used, e.g. as provided by [4]. Choose the initial guesses of $\mathbf{x}$ as $\frac{1}{\rho}[a, 1]$, $\frac{1}{\rho}[a, \frac{1}{5}]$ and $\rho[a, \frac{1}{5}]$. Numerical experiments have shown that using $\rho = 10$ will provide the true solution $\mathbf{x}_{cr}$ and σ_{cr}^R.

5. Choose σ_f^R as the least of σ_{tw}^R and σ_{cr}^R and calculate the failure index Φ from equation (11).

Numerical example with experimental validation

In the following, an example of corrugated board is analyzed with respect to material failure and structural failure. Experimental data from [6] is used for comparison of measured collapse stresses versus the failure stress calculated by (10). In the reference, experiments are performed on cylinders which dimensions are sized to avoid global buckling. Furthermore, the influence of structural failure on overall collapse of the corrugated board and the change of failure stress with varied wavelength of the fluting is investigated. The board dimensions and experimental data of stiffnesses and strengths of the facing material are presented in Table 1.

Table 1: Experimental data of the facing material.

Board dimensions [mm]	Data from Patel et. al. [6][a]
Thickness, h	0.248
Wavelength of fluting, a	7.2
Tensile and compressive strengths [MPa]	
X_t	85.7
X_c	25.2
Y_t	35.2
Y_c	14.7
Stiffness properties [GPa]	
E_{11}	8.36
E_{22}	3.41
G_{12}	2.06
G_{13}	0.045
G_{23}	0.045
ν_{12}	0.17

[a] Average values of inner and outer liner, see [6].

The tensile and compressive properties from Table 1 are used for the solution of equation (7) and the board dimensions and stiffness properties are used for solution of (8). The parameter α, for the given relation of $X_c/Y_c = 1.71$, is calculated to $\alpha = 0.78$, which yields the shear strength $T = 15$ MPa. Since the measured stress values from [6] are

based on average stresses between the facings, the figures in Table 1 are also averaged for use in the failure calculations.

In Figure 4 the failure stress is plotted in the compressive $\{\sigma_{11}, \sigma_{22}\}$-region, i.e. $\sigma_{12} = 0$, together with the measured collapse stress and the Tsai-Wu envelope. It can be seen that

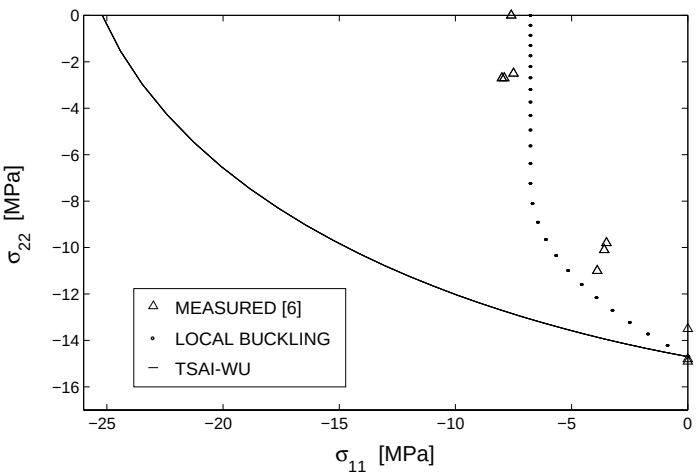

Figure 4: Failure stress in the compressive biaxial region, $\sigma_{12} = 0$.

the measured collapse stress fits very well to the failure stress radius, which is governed completely by local buckling in this stress region.

In Figure 5 the failure stress is plotted for combined shear and normal stress, i.e. σ_{22} versus σ_{12}. For this load combination it is seen that the failure stress radius is governed by material failure when the shear stress is large, and local buckling, or material failure, when the normal stress is large.

It may be useful to picture the failure stress radius for the general in-plane stress state, i.e. all stresses $\{\sigma_{11}, \sigma_{12}, \sigma_{22}\}$ non-zero. This is shown in Figure 6, where σ_{22} is plotted versus σ_{11} for various levels of σ_{12}. The shear stress levels are given as the outermost curve corresponding to the first value, $\sigma_{12} = 0$.

In Figure 7, the ratio of structural to material strength with decreasing fluting wavelength is plotted. A parameter η, defined by $a = a_0/\eta$, is used for lowering a from $a = a_0 = 7.2$ mm. The stress state is equibiaxial compressive, i.e. $\sigma_{11} = \sigma_{22}$, $\sigma_{11} \leq 0$ and $\sigma_{12} = 0$. This corresponds to the intersections of a straight line, forming 45 deg to the negative x-axis, and the curves corresponding to local buckling and Tsai-Wu failure in Figure 4. For values of $\eta \leq 1.4$, i.e. for $a \geq 5.1$ mm, the failure is seen to be governed by structural failure. At $a = 5.1$ mm, i.e. a 29% decrease of the fluting wavelength, the values of structural failure and material failure are equal. Note that for the stiffness parameters, typical for paper, a linear relation is found in Figure 7, i.e. $\sigma_{cr}^R \sim \frac{1}{a}$, while for isotropic thin plate bending a relation $\sigma_{cr}^R \sim \frac{1}{a^2}$ should be expected.

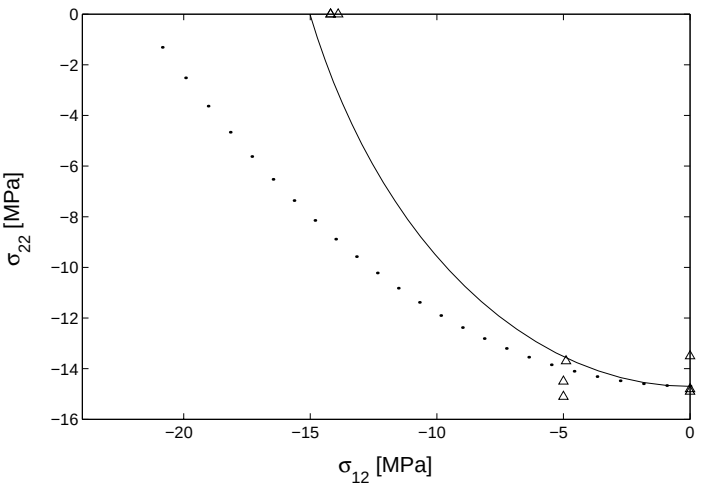

Figure 5: Failure stress in shear-compressive region, $\sigma_{11} = 0$.

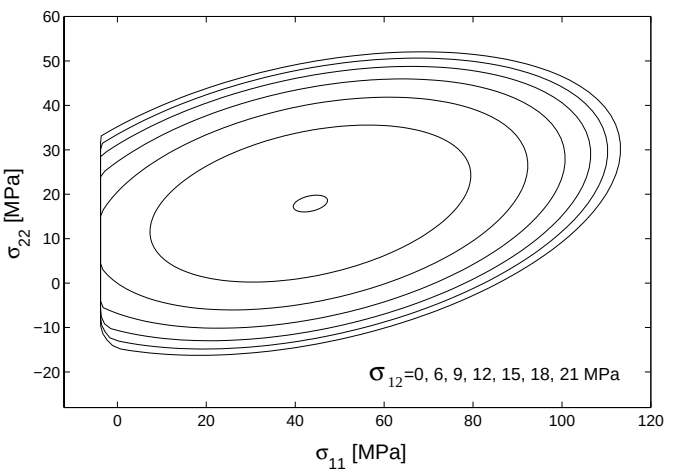

Figure 6: Failure stress for various shear levels.

Concluding remarks

A failure stress criterion for corrugated board facings has been presented. The criterion is based on material failure and structural failure, which are evaluated in a combined analysis procedure. The failure stress is compared with collapse experiments on corrugated board cylinders and the failure stress presented herein is seen to be in much better agreement with the measured stresses than the Tsai-Wu failure criterion alone. The procedure for finding the failure stress can be implemented in a finite element program for failure

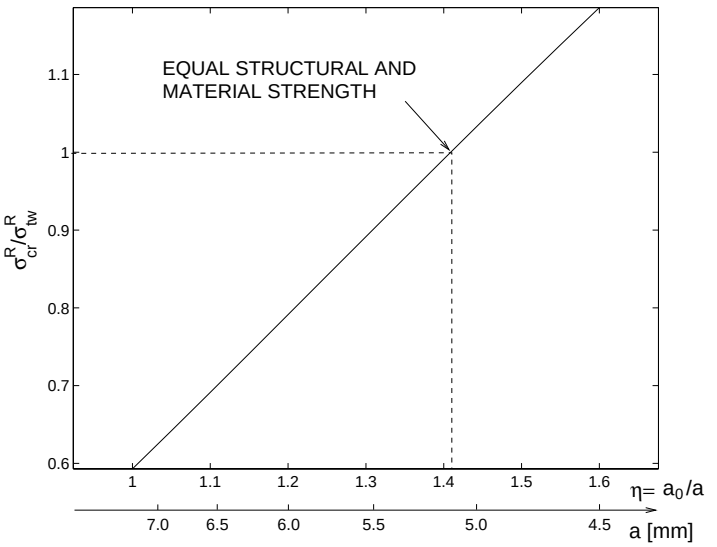

Figure 7: The ratio of structural to material strength with decreasing fluting wavelength for uniform biaxial compressive stress.

evaluation of e.g. corrugated containers.

Acknowledgements

The work herein was supported by "Bo Rydins stiftelse för vetenskaplig forskning" [The Bo Rydin Foundation for Scientific Research] and by FPIRC - Forest Products Industry Research College.

References

[1] C. Fellers, B. Westerlind and A. de Ruvo, *An Investigation of the Biaxial Failure Envelope of Paper: Experimental Study and Theoretical Analysis*. In Transaction of the Symposium, Cambridge, Vol. 1, pp. 527-559, (1983)

[2] P. J. Gustafsson, U. Nyman and S. Heyden, *A Network Mechanics Failure Criterion*. report TVSM-7128, Division of Structural Mechanics, Lund University, To be published

[3] M. W. Johnson and T. J. Urbanik, *Analysis of the Localized Buckling in Composite Plate Structures with application to Determining the Strength of Corrugated Fiberboard*. J. of Composites Technology and Research, Vol. 11, No. 4, pp. 121-127, (1989)

[4] MATLAB, *High Performance Numerical Computation and Visualization Software*. The Math Works Inc., Natick, Ma, USA, (1992)

[5] U. Nyman and P. J. Gustafsson, *Local buckling of corrugated board facings*. Proceedings of the European Conference on Computational Mechanics, Munich, Germany, (1999)

[6] P. Patel, T. Nordstrand, L. A. Carlsson, *Local Buckling and Collapse of Corrugated Board Under Biaxial Stress*. KFS AB, (1996)

[7] J. Tryding, *A Modification of the Tsai-Wu failure criterion of the Biaxial Strength of Paper*. Vol. 77, No. 8, Tappi Journal, (1994)

[8] S. W. Tsai and E. M. Wu, *A General Theory of Strength for Anisotropic Materials*. **5**, pp 58-80, J. Comp. Mater., (1971)

[9] J. J. Zahn, *Local Buckling of Orthotropic Truss-Core Sandwich*. Research paper, USDA Forest Service, (1973)

Paper 4

Multilayer Reliability Analysis of Corrugated Board

Ulf Nyman
Division of Structural Mechanics
Lund University

Multilayer Reliability Analysis of Corrugated Board

By Ulf Nyman[1]

ABSTRACT: The reliability of corrugated board is studied by finite element Monte Carlo simulations and by a first order reliability method, with the use of a failure criterion that includes both material failure and structural failure. The stiffness and strength parameters of the board are given as scalar multipliers of a geometrically distributed stochastic field. For the case of pure bending stresses, it is concluded that the failure is almost completely governed by structural failure. It is also seen that the board is very sensitive to compressive stresses in the machine direction (MD).

Introduction

The concept of reliability of engineering structures has focused increased attention during the last decades. In many applications one is interested in assessing the quality and safety of structures which may include strength and/or load variables that are represented by stochastic distributions. Basically, the establishment of structural reliability can be formulated by a limit state function, involving restrictions of a response quantity as well as the calculated response. The problem is devoted to determine the distribution parameters or the reliability index of the exceedance of structural strength to calculated response. The reliability index is a direct measure of the probability of failure.

Several methods are available for the settlement of the reliability index and the probability of failure. The methods can be classified as exact, e.g. Monte Carlo simulations (MCS), and approximative, e.g. First/Second Order Reliability Methods (FORM/SORM). In using the former example, a suitable number of samples are created as input variables to the structural model. The distribution for the limit state functions are then evaluated as the outcome from the MCS. In the latter example, the limit state functions are calculated in an iterative manner and the reliability index is directly obtained at the point of convergence. The usefulness of FORM/SORM is certainly expressed when the limit state function involves only a single performance quantity, for example the maximum displacement allowed at a generic point. Then, a reliability solution is achieved to a comparably low computational cost.

The treatment of the reliability of corrugated board, Figure 2, has received little attention so far. Previously, work has been devoted to deterministic calculations. The need for predicting the strength of packages/corrugated board has led to the development of various models in order to characterize the board, e.g. [2, 5, 6]. The aim of this paper is to present an analysis of corrugated board for which the reliability is studied by finite

[1]Structural Mechanics, Lund University, PO Box 118, S-221 00 Lund, Sweden.

element MCS and FORM. It is also the aim to investigate the applicability of FORM to finite element analysis in terms of accuracy, complexity and numerical efficiency. The report presented here is an extension of the work presented in [1], where only MCS was performed.

Variations in material parameters due to variations in strength variables such as moisture exposure is considered to affect the overall board performance. As stochastic variables are chosen the stiffness matrix components and the material directional strengths. A stochastic field is applied as a geometrical distribution of the variables. The failure criterion presented in [4], which was proven to provide an accurate agreement of the board failure compared to test data, is used in the settlement of the limit state functions. In the analysis, the variation of the probability of failure due to different extent of correlation at a certain length, is examined. Furthermore, studies of the likeliness of failure at specific geometrical points of the board are performed.

Limit state functions

The failure of corrugated board is assumed to take place in either of the facings. Studies of the board behaviour [2, 8, 9] prior and at the moment of collapse strongly indicates that the failure is influenced by local stability. In [4] a combined failure criterion was developed, based on the calculation of a failure stress radius. From a sandwich plate stress estimation, a failure mode evaluation can be done whether the failure stress radius is due to material or structural failure. For the stress state in an outer layer, a limit state function can be formulated for each random field element i as

$$g(\boldsymbol{\alpha}_i) = \sigma_f^R(\boldsymbol{\alpha}_i) - \sigma^R(\boldsymbol{\alpha}_i) \leq 0 \tag{1}$$

where σ^R is the evaluated stress radius, σ_f^R is the failure stress radius and $\boldsymbol{\alpha}_i$ are the stochastic variables.

Structural failure surface

If the number of elements is large, or a large amount of simulations are performed, the calculation of the structural failure stress radius may be costly. However, from [4] it was concluded that most of the part of the surface defining structural failure, interior material failure, is a plane surface. In [1], the failure due to instability was given by the stress plane corresponding to a constant stress $\sigma_{11} = k_{cr}$ in the first direction (MD). This is the critical stress corresponding to uniaxal structural failure. An explicit expression for k_{cr} is then found as the limit value

$$k_{cr} = \lim_{\lambda \to \infty,\, \mu = 0} \sigma^R(\mathbf{n} = [-1, 0, 0]), \quad k_{cr} < 0 \tag{2}$$

where $\mathbf{n}$ is the directional stress vector, $\mathbf{n} = [n_{11}, n_{12}, n_{22}]$ (unit vector), and λ and μ are the half buckling wavelength in the second direction (CD) and slope of nodal lines [4], respectively. Then the critical stress radius is given by

$$\sigma_{cr}^R = \frac{k_{cr}}{n_{11}}, \quad \sigma_{cr}^R > 0 \tag{3}$$

However, in a reliability analysis using minimization algorithms, the open failure surface defined by (2) might cause numerical problems when the initial search values are chosen far apart from the minimum distance point. Therefore, the plane is substituted for by a quadratic closed surface according to

$$(\sigma_{11} - b)^2 + \sigma_{12}^2 + \sigma_{22}^2 = R^2 \tag{4}$$

where R is assigned some large value and b should be given so as to fulfil

$$R - b = |k_{cr}|, \quad R > b \tag{5}$$

Since n_{11} is less than zero for structural failure to take place, and σ_{cr}^R must be positive, the critical stress radius is given by

$$\sigma_{cr}^R = bn_{11} + \sqrt{b^2 n_{11}^2 + R^2 - b^2} \tag{6}$$

It is worth noting that the larger R is chosen, the more (6) will approach (3). However, in order not to create a badly conditioned problem, R should be chosen as a reasonable factor of $|k_{cr}|$, for example as $R = 5|k_{cr}|$.

Finite element response

In the solution of the reliability index for a given material point, or random field element, it is required to achieve the gradient of (1) at each iteration point in the minimization procedure. This involves the calculation of the stresses as function of the stochastic variables, which could be achieved by a series expansion of the response variables. In this work, however, the determination of the gradients of the limit state function is performed by the full finite element solution, i.e. numerically. The procedure is to solve $\mathbf{a}^{(k)}(\boldsymbol{\alpha}_i)$ from

$$\mathbf{K}^{(k)}(\boldsymbol{\alpha}_i)\mathbf{a}^{(k)}(\boldsymbol{\alpha}_i) = \mathbf{f}^{(k)}(\boldsymbol{\alpha}_i) \tag{7}$$

at the iteration points k. The stresses are then given by

$$\boldsymbol{\sigma}^{(k)}(\boldsymbol{\alpha}_i) = \mathbf{D}^{(k)}(\boldsymbol{\alpha}_i)\boldsymbol{\varepsilon}^{(k)}(\boldsymbol{\alpha}_i) = \mathbf{D}^{(k)}(\boldsymbol{\alpha}_i)\mathbf{B}\mathbf{a}^{(k)}(\boldsymbol{\alpha}_i) \tag{8}$$

from where the failure stress radius can be calculated for evaluation of the limit state function.

The solution of (7) is obtained as the Cholesky decomposition of $\mathbf{K}^{(k)}$

$$\mathbf{K}^{(k)} = \left(\mathbf{G}\mathbf{G}^T\right)^{(k)} \tag{9}$$

where $\mathbf{G}$ is a lower triangular matrix. Further on, $\mathbf{a}^{(k)}$, can be determined by the solution of the triangular systems

$$\begin{aligned} \mathbf{G}^{(k)}\tilde{\mathbf{a}}^{(k)} &= \mathbf{f}^{(k)} \\ \left(\mathbf{G}^T\right)^{(k)}\mathbf{a}^{(k)} &= \tilde{\mathbf{a}}^{(k)} \end{aligned} \tag{10}$$

It is interesting to observe that, if the load variables are the only variables that contain uncertainties, the stiffness matrix will not change during the iterations and the Cholesky decomposition in (9) needs to be done only initially. This is attractive in terms of the computation time required for the iteration process.

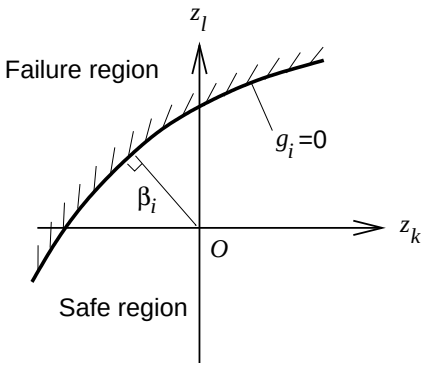

Figure 1: Relibility index in z-coordinate system.

FORM procedure for calculation of reliability indices

For reasons that will be obvious in the next section the basic variables will now be denoted as $\mathbf{x}$, instead of $\boldsymbol{\alpha}$ as before. Initially, the basic variables, $\mathbf{x}$, may not be normally distributed. In a FORM procedure, it is required that the variables $\mathbf{x}$ are transformed from the initial ditribution to an equivalent normal distribution. This can be done approximately, e.g. by the transformation given by Rackwitz and Fiessler [11]. If the basic variables are log-normally distributed, an exact mapping is possible by using

$$\mathbf{y} = \log \mathbf{x} \tag{11}$$

and determining the parameters

$$\begin{aligned} \mathrm{E}[y_i] &= \log\left(\mathrm{E}[x_i] - \frac{1}{2}\mathrm{Var}[y_i]\right) \\ \mathrm{Var}[y_i] &= \log\left[\left(\frac{\mathrm{Var}[x_i]}{\mathrm{E}[x_i]}\right)^2 + 1\right] \end{aligned} \tag{12}$$

respectively the correlation matrix components

$$\rho_{ij}^{(y)} = \log\left(1 + \rho_{ij}^{(x)} V_{x_i} V_{x_j}\right) \left(\log\left(1 + V_{x_i}^2\right) \log\left(1 + V_{x_j}^2\right)\right)^{-1/2} \tag{13}$$

where V_x is the coefficient of variation of $\mathbf{x}$.

The basic idea in using FORM is to use a reliability index β, see Figure 1, which is invariant of a coordinate system rotation. This is accomplished by a mapping of the stochastic variables according to Hasofer and Lind, [13],

$$\mathbf{z} = \hat{\mathbf{C}}_y^{-1/2} \left(\hat{\mathbf{y}} - \mathrm{E}[\hat{\mathbf{y}}]\right) \tag{14}$$

where $\hat{\mathbf{y}}$ are the uncorrelated normal distributed variables. The variables $\hat{\mathbf{y}}$ are chosen mutually independent by the orthogonal transformation matrix $\mathbf{A}$

$$\hat{\mathbf{y}} = \mathbf{A}^T \mathbf{y} \tag{15}$$

so that

$$\mathrm{E}[\hat{\mathbf{y}}] = \mathbf{A}^T \mathrm{E}[\mathbf{y}] \tag{16}$$

and $\hat{\mathbf{C}}_y$ is a diagonal matrix

$$\hat{\mathbf{C}}_y = \mathbf{A}^T \mathbf{C}_y \mathbf{A} \tag{17}$$

where $\mathbf{C}_y$ is the covariance matrix of $\mathbf{y}$.

In evaluating the limit state function in the original coordinate system, the basic variables $\mathbf{x}$ needs to be determined. By using (14) and (15), the following is obtained

$$\mathbf{y} = \mathbf{A}\hat{\mathbf{y}} = \mathbf{A}\left(\hat{\mathbf{C}}_y^{1/2}\mathbf{z} + \mathrm{E}[\hat{\mathbf{y}}]\right) = \mathbf{A}\left(\hat{\mathbf{C}}_y^{1/2}\mathbf{z} + \mathbf{A}^T\mathrm{E}[\mathbf{y}]\right) \tag{18}$$

From (18) the basic variables $\mathbf{x}$ are then determined as

$$\mathbf{x} = \mathrm{e}^{\mathbf{y}} \tag{19}$$

In an iteration procedure, of course, the eigenvalues of $\mathbf{C}_y$ needs to be determined only initially.

The reliability index is determined as the point of convergence, the minimum distance from the origin to the point $\mathbf{z}^*$ in the z-coordinate system, from a sequence of the iteration points, $\mathbf{z}^{(k)}$. For a general limit state surface, an approximation of the probability of failure, P_f, is given by

$$P_f = \Phi(-\beta_i) \tag{20}$$

where Φ is the standard normal distribution function and β_i is the reliability index of a generic material point i.

When the system failure is analyzed, as in the case of a structure discretisized by finite elements, the failure probability is determined for all points of prospective failure, as given by the random field discretization. The system failure can be chosen as the union of failures for a series system, and the probability of failure can be given between upper and lower bounds, [12]. The calculation of the bounds uses the two-fold joint probabilities of failures, P_{ij}.

At the design point, the linearized limit state function is given by

$$g_i^* = \sum_{k=1}^{n} \frac{\partial g_i(z^*)}{\partial z_k}(z_k - z_k^*) = 0 \tag{21}$$

which can be rewritten on normal form

$$g_i^* = \frac{1}{\left[\sum_{k=1}^{n}\left(\partial g(z^*)/\partial z_k\right)^2\right]^{1/2}} \sum_{k=1}^{n} \frac{\partial g(z^*)}{\partial z_k} z_k + \beta_i = 0 \tag{22}$$

or

$$g_i^* = \sum_{k=1}^{n} a_{ik} z_k + \beta_i = 0 \tag{23}$$

The linearized limit state functions g_i^* and g_j^* are standard normally distributed with correlation coefficient ρ_{ij}. The correlation coefficient is given as

$$\rho_{ij} = \sum_{k=1}^{n} a_{ik} a_{jk} \tag{24}$$

Then, the joint probability of failure, P_{ij}, can be determined from the numerical integration of

$$P_{ij} = \int_{-\infty}^{-\beta_i} \int_{-\infty}^{-\beta_j} \varphi(x, y; \rho_{ij}) dx dy \tag{25}$$

where $\varphi(x, y; \rho_{ij})$ is the joint standardized normal probability density function.

Random field representation

In addressing the safety of the corrugated board, subjected to any kind of load, it is crucial to identify a set of variables that incorporate uncertain properties. In this case the purpose is to analyze a physical variation of moisture exposure of the board. It is known that both the strength and stiffness of paper change drastically when subjected to moisture. It can also be concluded that strong correlation exists between the variation in strength and stiffness. Therefore, in order to reduce the number of stochastic variables to a reasonable amount, the strength and stiffness variables $\boldsymbol{\alpha}$ can be chosen as a scalar multiplier to a spatially distributed variable, $\mathbf{x}$ so that for a given geometric point i

$$\boldsymbol{\alpha}_i = \mathbf{c} x_i \tag{26}$$

In this case, for example the stiffness and material tensile strength the in first direction are determined by

$$E_{11}^{(i)} = C_{E_{11}} x_i, \quad X_t^{(i)} = C_{X_t} x_i \tag{27}$$

respectively. The constants $C_{E_{11}}$ and C_{X_t} are the measured parameters under normal conditions. Other stiffness and material strength parameters, assumed to be orthotropic, are made proportional to $E_{11}^{(i)}$ and $X_t^{(i)}$, respectively. Poissons ratio is assumed to be deterministic in this case. The matrix defining the covariance over the plate region is defined by

$$C_{ij} = \begin{bmatrix} \mathrm{Var}[x_1] & \mathrm{Cov}[x_1, x_2] & \dots & \mathrm{Cov}[x_1, x_n] \\ \mathrm{Cov}[x_2, x_1] & \mathrm{Var}[x_2] & \dots & \mathrm{Cov}[x_2, x_n] \\ \vdots & \vdots & \ddots & \vdots \\ \mathrm{Cov}[x_n, x_1] & \mathrm{Cov}[x_n, x_2] & \dots & \mathrm{Var}[x_n] \end{bmatrix} \tag{28}$$

where n is the number of stochastic variables. The covariance between the two points, i and j, at a distance D_{ij} from each other, is taken as

$$C_{ij} = (\mathrm{Var}[x_i]\mathrm{Var}[x_j])^{1/2} \rho_{ij} = (\mathrm{Var}[x_i]\mathrm{Var}[x_j])^{1/2} \, \mathrm{e}^{-D_{ij}/L} \tag{29}$$

where ρ_{ij} is the correlation coefficient between the points and $L = -D^*/\log \rho^*$. ρ^* is the value of correlation between two points at distance D* from each other. The distance D_{ij} can be obtained as

$$D_{ij} = \|\mathbf{v}\| \tag{30}$$

where $\mathbf{v}$ is the geometric vector between the points, here chosen as the midpoints of the random field elements.

Finite element model

In the calculations of the structural response the finite element toolbox CALFEM [7] is used. The bending behaviour is modelled by a quadrilateral multilayered composite plate element, see Figure 2, using bi-linear interpolation functions for the nodal quantities.

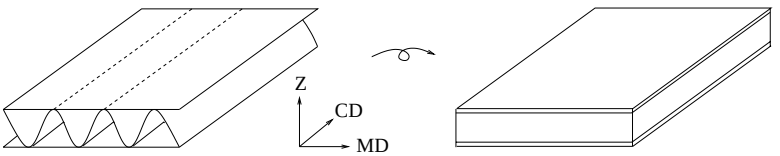

Figure 2: Finite element model of corrugated board.

In determining the effective elastic modulus of the core the procedure described in [3] is used. The counterpart element sides are parallel to each other which enables the stiffness matrix to be determined analytically. The thickness integration part of the stiffness matrix is given by

$$\tilde{\mathbf{D}} = \int_{-h/2}^{h/2} \mathbf{D}(z) z^2 dz \tag{31}$$

where $\mathbf{D}(z)$ is the in plane orthotropic material matrix in the current layer. The matrix $\mathbf{D}$ must be calculated for each layer and element for every new set of values of $\boldsymbol{\alpha}_i$.

Based on the curvature, $\boldsymbol{\kappa}$, the stresses in layer k are determined from

$$\boldsymbol{\sigma}^{(k)} = -z^{(k)} \mathbf{D}^{(k)} \boldsymbol{\kappa} \tag{32}$$

where $z^{(k)}$ is the distance from the plate system line to the center line of the layer.

Numerical results

The system reliability of a simply supported composite plate, subjected to a surface normal pressure, is studied. The plate is quadratic with side dimension 0.5 m. The middle layer is assigned deterministic values and assumed only to contribute with bending stiffness along the corrugations. An effective Young's modulus of the middle layer is calculated by multiplying the paper modulus with $\gamma t_2/h_2$, see [3], where γ is the ratio of the corrugated wave intrinsic length to the wavelength. Moreover t_2 and h_2 is the paper and core thickness, respectively. The value of h_2 is 3.6 mm and the paper thicknesses for all three layers are 0.248 mm. The wavelength of the core corrugations is 7.2 mm, which yields $\gamma \sim 1.4$.

The material parameters of the paper material, referred to as C_E and C_X previously, are used as scalar multipliers to the distribution variables x_i. The values for the stiffness parameters are $C_{E_{11}} = 8.36$, $C_{E_{22}} = 3.41$, $C_{G_{12}} = 2.06$, and $C_{G_{13}} = C_{G_{23}} = 0.045$ GPa. The in plane Poissons ratio is $\nu_{12} = 0.17$. Furthermore, the tensile and compressive material strengths in the first direction is $C_{X_t} = 85.7$ and $C_{X_c} = 25.2$ MPa respectively, and in second direction $C_{Y_t} = 35.2$ and $C_{Y_c} = 14.7$ MPa. The shear strength is obtained as proposed in [10].

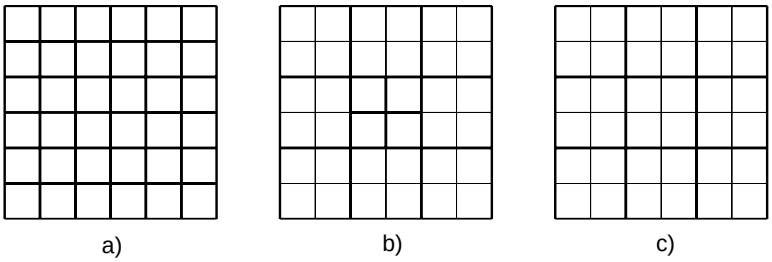

Figure 3: Different resolutions of the random field mesh.

An isotropic probabilistic distribution for the geometric variables x_i is assumed. The distribution for x_i is taken to be log-normal with mean $\mathrm{E}[x_i] = 1$ and variance $\mathrm{Var}[x_i] = 0.09$. It should be noted that in [1], a normal distribution, truncated at zero, was chosen for the geometric variables. However, it was observed that for the case of using FORM, this led to numerical problems in terms of a singular stiffness matrix. The reason for this is that the modulus of elasticity is a strength variable in the case of structural failure. For the low amount of load applied, yielding small values of the probabilities of failure, this results in strength variables tending to be very small, i.e. close to zero, in the iteration procedure.

Two numerical examples are examined. The first example is a comparison of MCS and FORM. Three different types of random field meshes are investigated in the FORM procedure, see Figure 3 where the random field elements are drawn with bold lines. In case (a) the random field elements are coinciding with the finite elements, in case (b) 12 random field elements are used and in case (c) 9 random field elements are used. In addition, a case (d), with the same random field mesh as in (a) but with a reduced number of searches for the reliability index, is investigated. In this case, only the elements with a deterministic ratio of the stress radius to the failure stress radius of 0.3 is used in the search (the four center elements along with their neighbour elements, corner elements excluded). At all MCS, the random field mesh is coinciding with the finite element mesh.

Also the variation of probability of failure due to different extent of correlation at a certain length, is investigated. A surface pressure of 175 Pa is applied on each element, which results in a maximum deterministic deflection of 4.5 mm, see Figure 4.

The second example uses MCS to study the likeliness of failure at specific geometrical points of the board. Here, a larger surface pressure is applied, 500 Pa. The values of D^* and ρ^* are both 0.5.

In the first example the correlation between the geometric variables is varied. This is accomplished by calculating the probability content for values of ρ^*=0.01 to ρ^*=0.9. The result is plotted in Figure 5, where the circles are results from MCS and the solid lines are results from FORM. The failure probability increases with increasing correlation length and takes the value 0.0017 when all the elements are strongly correlated. This is quite lower than the value obtained in [1], even though the surface pressure applied is larger. The reason for this is the low density function values for the log-normal distribution, for the level of the applied load. However, it can be seen that the results from MCS and FORM are very close.

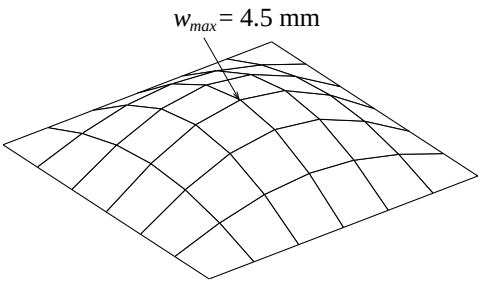

Figure 4: Deflection of composite plate.

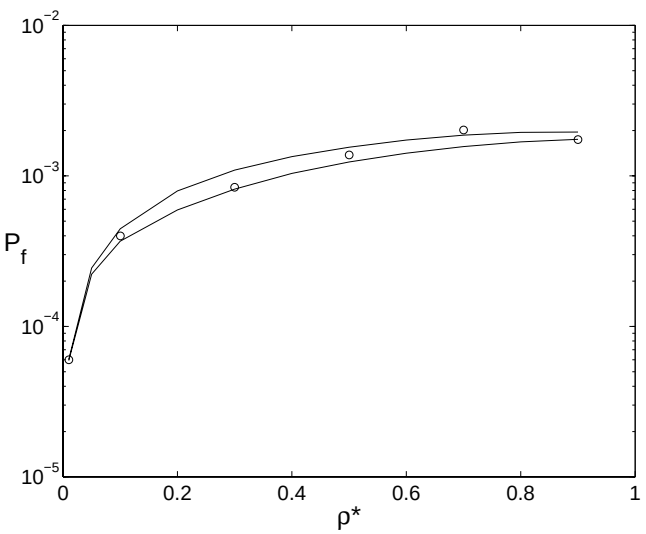

Figure 5: P_f as function of correlation length coefficient.

In Table 1, the results from the three different random field meshes are listed, where the probabilities of failure are given as the mean value of the upper and lower bounds. The value of ρ^* is 0.5 in all cases.

Table 1: Probability of failure for different random field meshes.

	MCS	FORM			
		a	b	c	d
Prob. of failure, 10^{-3}	1.38	1.30	0.77	0.51	1.30
No. Chol. decomp.	50000	8695	936	570	2220

It is seen that when the random field mesh is coinciding with the finite element mesh, the number of required Cholesky decompositions is 8695, for the FORM solution, compared to 50000 for the MCS solution. Furthermore, the probability of failure is a little less than for the case of MCS. For the random field mesh (b) the probability of failure is far from the value in case (a), which indicates that the random field discretization is to coarse. The same holds for case (c). In case (d), however, the reduced number of search elements do not deteriorate the result from (a), where the probability of failure is the same, 0.0013. The number of Cholesky decompositions needed for FORM in (d) is 2220.

It can be concluded from the cases (a)-(d) that the number of random field elements, and thereby the number of stochastic variables, largely affects the rate at which a solution is obtained for the probability of failure. In case (d) the number of search points was 12, the same as the number of random field elements in (b). Despite this, the number of required Cholesky decompositions is more than twice than in case (b).

In the second example the number of fractures in each layer, element and whether the failure is due to structural or material failure, is determined. The number of simulations is 50000. It was noted during the simulations that no failures in the upper layer occurred (where tensile stresses are developed). It should be noted that in [1], where normal distributed variables where used, a few number of failures occured in the upper layer.

In Figure 6, the numbers in braces are failures due to material failure. As can be seen, material failure only develop in the corner elements, where the shear stress is large. In addition, it can be seen that the number of failures in regions where the curvature in MD is larger compared to CD, exceeds the number of failures in regions where the oppostite holds for the curvature. As a conclusion, the board is more sensitive to compressive stresses in MD, than in CD. This result was also confirmed in [1], where an added tensile stress in the MD largely reduced the number of structural failures at the compressive side of the plate.

Conclusions

The reliability of corrugated board, subject to plate bending, is studied both by MCS and by a FORM procedure applied to finite element calculations. The stiffness and strength parameters of the board are given as scalar multipliers of a geometrically distributed stochastic field.

{1}	5	7	6	6	
18	7609	17274	17230	7399	19
82	21987	36545	36441	21994	86
74	22084	36582	36385	22056	94
11	7422	17427	17303	7449	22
{1}	6	8	8	3	{1}

Figure 6: Number of failures in each element.

For the case of pure bending stresses, it is concluded that the failure is almost completely governed by structural failure. It is also seen that the board is sensitive to stresses in the first direction (MD).

Also the variation of probability of failure due to different correlation lengths is studied. The system failure probability is seen to increase with increasing correlation length coefficient.

With the use of MCS, it is recognized that a very large number of Cholesky decompositions is needed for determining the probabilistic characteristics of the board. This is certainly expressed when low failure probabilities are studied. The method of FORM was shown to be a numerically efficient method, even though the failure surface is not explicitly given, but determined by the finite element solution. It should be noted that the response gradients could have been calculated analytically, thus saving a lot of computation time. However, the calculations done here shows that even if the gradients are computed by the full finite element solution, there is significant computational effort to save. This is also attractive since general purpose FEM codes could be used together with FORM without modifications.

It should be mentioned that the example studied here consists of rather few elements representing the structure. If larger problems are studied, and the correlation between each element is high, there could arise problems with widening reliability bounds for the system failure.

In analysing corrugated board in a broader sense, as in the case of currugated board packages, a very common load case is in-plane loaded panels. A detailed analysis would require a geometrically non-linear finite element analysis. Studying the reliability of e.g. boxes by MCS, this would lead to a prohibitive computational effort needed. A possible choice would be to extend the limit surface iterations to involve also equilibrium iterations in a buckling analysis.

Acknowledgements

The economic support for this work from the Foundation for Strategic Research (SSF) Forest Products Industry Research College program and from Bo Rydins stiftelse för vetenskaplig forskning is gratefully acknowledged.

References

[1] Nyman, U., and Gustafsson, P. J., (2000) *Multilayer Composite Reliability Calculations on Corrugated Board*, Proceedings of the International Conference on Wood and Wood Fiber Composites, April 13-15, Stuttgart, Germnany

[2] Johnson, M. W. and Urbanik, T. J. (1989): Analysis of the Localized Buckling in Composite Plate Structures with application to Determining the Strength of Corrugated Fiberboard. J. of Composites Technology and Research, Vol. 11, No. 4, 121-127

[3] Nordstrand, T. M. (1995): Parametric Study of the Postbuckling Strength of Structural Core Sandwich Panels. Composite Structures, 30, 441-451

[4] Nyman, U. and Gustafsson, P. J. (2000) Material and Structural Failure Criterion of Corrugated Board Facings. Accepted for publication in Composite Structures.

[5] Patel, P. (1996): Biaxial Failure of Corrugated Board. KFS AB, Lund

[6] Urbanik, T. J. (1997): Linear and Nonlinear Effects on Postbuckling Strength of Corrugated Containers. Mechanics of Cellulosic Materials, AMD-Vol. 221/MD-VOI. 77, ASME

[7] CALFEM 3.3, (1999): A finite element toolbox to MATLAB, Jabe Offset AB, Division of Structural Mechanics, Lund University

[8] Patel, P., Nordstrand T. M. and Carlsson, L. A. (1997): Local Buckling and Collapse of Corrugated Board Under Biaxial Stress. Composite Structures, Vol. 39, No 1-2, 93-110

[9] Zahn, J. J. (1973): Local Buckling of Orthotropic Truss-Core Sandwich. Research paper, USDA Forest Service

[10] Gustafsson, P. J., Nyman, U. and Heyden, S. (2000): A network mechanics failure criterion. Report TVSM-7128, Division of Structural Mechanics, Lund University

[11] Rackwitz, R., and Fiessler, B., (1977): An algorithm for Calculation of Structural Reliability under Combined Loading. Berichte zur Sicherheitstheorie der Bauwerke, Lab. f. Konstr. Ingb., Munchen

[12] Ditlevsen, O., (1979): Narrow Reliability Bounds for Structural Systems. J. Struct. Mech., Vol. 7, pp. 435-451

[13] Hasofer, A. M, and Lind, N. C., (1974): An Exact and Invariant First Order Reliability Format. Proc. ASCE, J. Eng. Mech. Div., pp 111-121